# Selective autophagy fine-tunes Stat92E activity by degrading Su(var)2-10/PIAS during glial injury signalling in *Drosophila*

Virág Vincze[1,2], Zsombor Esküdt[1,3,4], Erzsébet Fehér-Juhász[1], Aishwarya Sanjay Chhatre[1,2], András Jipa[1], Martin Csordós[1,5], Anna Rita Galambos[1], Dalma Börcsök[1], Gábor Juhász[1,6]* and Áron Szabó[1]*

Affiliations

1. HUN-REN Biological Research Center, Institute of Genetics, H-6726 Szeged, Hungary
2. Doctoral School of Biology, University of Szeged, H-6726 Szeged, Hungary
3. National Academy of Scientist Education Program of the National Biomedical Foundation, Szeged, H-6721, Hungary
4. Albert Szent-Györgyi Medical School, University of Szeged, Szeged, H-6720, Hungary
5. Faculty of Science and Informatics, University of Szeged, Szeged, H-6726, Hungary
6. Department of Anatomy, Cell and Developmental Biology, Eötvös Loránd University, Budapest, H-1117, Hungary

*Correspondence to: aszabo@brc.hu, juhasz.gabor@brc.hu

## Abstract

Glial immunity plays a pivotal role in the maintenance of nervous system homeostasis and responses to stress conditions, including neural injuries. In *Drosophila melanogaster*, the transcription factor Stat92E is activated in glial cells following central nervous system injury, independently of the canonical JAK/STAT pathway, to shape glial reactivity towards degenerated axons. However, the upstream regulatory mechanisms governing Stat92E activation remain elusive. Here, we reveal a selective autophagy-mediated regulation of Stat92E in glia by the degradation of the Stat92E repressor Su(var)2-10, a member of the PIAS SUMO ligase family. Atg8a, a core autophagy factor co-localizes and interacts with Su(var)2-10. Su(var)2-10 elimination is required for efficient Stat92E-dependent transcription after

injury. Furthermore, we demonstrate that autophagy is essential for the upregulation of immune pathways, exemplified by *virus-induced RNA 1* (*vir-1*), in glial cells following axon injury. We propose that Stat92E function is gated both by activating phosphorylation and autophagic Su(var)2-10 breakdown to licence glial reactivity. These findings underscore the critical role of autophagy in glial immunity and its potential impact on neural injury responses.

## Introduction

The brain tissue in homeostatic conditions is constantly monitored by glia to mount an enhanced response in face of a challenge. Microglia persistently sample the environment with elongated processes looking for signals emitted from dying, damaged or infected cells. These trigger morphological and signalling changes in them to induce a transformation into a reactive state. Astrocytes undergo a similar transition upon stimuli. Reactive glia have distinct transcriptional signatures as exemplified by disease-associated microglia in neurodegeneration[1]. They sense damage- and pathogen- associated molecular patterns (DAMPs and PAMPs), find-me and eat-me cues via dedicated receptors to mount an immune response. They also release various chemokines and cytokines to spread and control neuroinflammation[2]. Upon central nervous system (CNS) injury, these receptors trigger signalling events that include MAPK, JAK-STAT and NF-κB pathways[2]. The transcriptomic changes in reactive glia show a great contribution from these signalling networks[3–7].

The JAK-STAT pathway is an important but less studied part of glial immunity, especially compared to the NF-κB pathway[8]. Most interleukin and interferon receptors signal through the JAK-STAT pathway in mammals and induce the expression of either pro- or anti-inflammatory cytokines depending on the STAT paralog, both in peripheral immune cells and in glia[8,9]. In neurodegenerative diseases, the JAK-STAT pathway contributes to neuroinflammation. Increased interferon-dependent microglial Stat1 activation is observed in models of Alzheimer's disease, causing complement-dependent synapse elimination[10].

Research on *Drosophila* has elucidated key early responses to axon injury in glia[11–15] with the single STAT transcription factor, Stat92E driving upregulation of the *draper* (*drpr*), the main phagocytic receptor in glia and the matrix metalloproteinase *Mmp1* to induce glial reactivity[16,17]. Interestingly, this response does not rely on canonical pathway components such as the JAK kinase (Hopscotch (Hop) in flies) or the upstream receptor Domeless (Dome)[16]. Instead, the Drpr receptor and its downstream signalling partners culminating in Rac1 activation

are required for glial Stat92E activation after injury[16]. Insulin-like signalling has also been shown to promote glial Stat92E activity[18]. How Rac1 relays signalling to Stat92E is not known[19]. However, besides Stat92E, the transcription factor AP-1 has also been shown to be required for *drpr* upregulation[12], and Draper/Stat92E/AP-1 activity contributes to proper *Mmp1* expression after axon injury[17].

Autophagy (more specifically macroautophagy) is a membrane-limited intracellular degradation pathway that removes cytoplasmic components including protein aggregates and organelles[19]. Autophagy initiation depends on the Atg1 (ULK1/2) complex. Upon induction by starvation or other stress conditions, nucleation process prepares membranes for vesicle formation. Along with Atg8a conjugation, a cup-shaped phagophore forms around the cargo and engulfs in by closing it into an autophagosome. Atg8a conjugation depends on two ubiquitin-like conjugation systems, Atg8a being lipidated by the Atg16/Atg5-Atg12 complex. Autophagosomes fuse with lysosomes where the cargo is broken down and recycled.

A targeted and precise variation on this theme is selective autophagy. During this process, cargo receptors recognize specific cellular components ranging from organelles to single molecules and recruit the autophagosome biogenesis machinery, irrespective of nutritional status[20,21]. Cargo receptors can bind to ubiquitylated material or are embedded in organelles, but labile molecules can also feature receptor-like motifs for direct degradation.

Stat92E activation being pivotal to glial adaptation to challenges, we need to gain a better insight into its regulatory mechanisms. In *Drosophila* glia, immediate upstream regulation of Stat92E activation upon injury is not well understood. Here we show that autophagy clears the direct Stat92E repressor PIAS/Su(var)2-10 in wing glia after wing transection thereby gating Stat92E-dependent transcriptional responses. Interestingly, *drpr* expression is not responsive to injury in these peripheral glial types, instead *vir-1*, another Stat92E target is induced after wing transection in an autophagy-dependent manner.

## Results

### Selective autophagy is necessary for Stat92E but not for JNK pathway activation

In an effort to understand nervous system adaptation to altered physiology after injury, we investigated whether autophagy impacts signalling pathways in glia. Two well-characterized immune pathways in glial responses are the JAK-STAT and the JNK pathways. We used a *Drosophila* wing injury model[22,23] (Fig. S1A) to measure transgenic reporter upregulation for both pathways. As in the antennal lobe of the brain after antennal ablation[11,12,16], the Stat92E

reporter *10xStat92E-GFP*[24] and the AP-1 reporter *TRE-EGFP*[25] both showed robust activation after injury in the wing nerve (Fig. 1A,B, S1B,C). This expression pattern coincided with glially driven myr::tdTomato signal (Fig. S1B,C), similarly to the glial upregulation of Stat92E and AP-1 reporters in the CNS. In order to establish the dynamics of *10xStat92E-GFP* upregulation in the wing nerve, we tested the GFP reporter intensity at different time points after injury (Fig. S1D,E). As 10xStat92E-GFP signal intensity reached its peak 3 days post wing injury (3 dpi), we measured the reporter activation levels 3 dpi hereafter. We then depleted *Atg16*, a core autophagy factor, specifically in glia using *repo-Gal4*. While *Atg16* silencing did not affect *TRE-EGFP* expression, it abrogated *10xStat92E-GFP* activation after injury (Fig. 1A-C). We also measured the Stat92E reporter activity in *Atg5 (Atg5$^{5cc5}$)* and *Atg8a (Atg8a$^{\Delta 12}$)* null-mutant (Fig. S2A) backgrounds, observing a comparable effect to the *Atg16* knockdown (KD) (Fig. 1D-F). This lack of activation could be rescued by an endogenous promoter-driven *Atg5* transgene (*Atg5::3xHA*) in the *Atg5*-deficient background (Fig. 1D,F).

Atg5, Atg8 and Atg16 are not only involved in autophagy but also in autophagy-related processes including LC3-associated phagocytosis (LAP), which we characterized in glia during axon debris degradation in glia[26]. Therefore, we set out to distinguish the contribution of these two processes to Stat92E signalling. Atg13 is a specific component of the autophagic machinery as part of the autophagy initiation complex which does not participate in LAP. *Atg13* silencing in glia abrogated Stat92E reporter activation (Fig. 2A,C). Unlike Atg13, Rubicon is not involved in autophagy, but it is required for LAPosome formation during LC3-associated phagocytosis. In contrast to *Atg13* knockdown, *Rubicon* RNA interference (RNAi) did not lead to loss of Stat92E activation (Fig. 2B,D). We conclude that canonical autophagy but not LAP sustains Stat92E signalling in glia.

We aimed to further investigate how autophagy specifically impacts Stat92E activation. Through their LC3-interacting region (LIR), selective autophagy receptors (SARs) bind the LIR motif docking site (LDS) on the core autophagy protein Atg8a. SARs directly interact with to-be-degraded cargos or with ubiquitin (Ub) chains on cargos. LIRs can be also present in cargos themselves leading to degradation via Atg8a. We evaluated a mutant that specifically removes the Atg8a LDS, for Stat92E-dependent gene activation[27]. *Atg8a$^{K48A/Y49A}$* (*Atg8a$^{LDS}$)* prevented Stat92E reporter upregulation following injury (Fig. 2E,F). Although silencing *ref(2)p/p62*, the best known Ub chain-binding SAR in *Drosophila* also showed a mild decrease in GFP reporter intensity, it eventually had no significant effect on *10xStat92E-*

*GFP* activation (Fig. S2B,C). Interestingly, bulk autophagic degradation in glia does not change in response to injury when we assay mCherry+ (lysosomal) versus mCherry+ GFP+ (non-lysosomal) puncta abundance of the tandem tag autophagic flux reporter mCherry-GFP-Atg8a directed into wing glia[28] (Fig. S2D). Considering the degradative function of autophagy, this suggests the removal of a negative Stat92E signalling regulator by selective autophagy, mediated mainly by a factor other than Ref(2)P/p62.

**Su(var)2-10 depletion enhances Stat92E activation in glia after wing injury**

We screened Stat92E repressors and upstream kinases for a potential to repress Stat92E in glia. As the upstream components of the JAK-STAT pathway, hop and Dome are not involved in glial injury responses in flies[16], we focused on interactors of Stat92E itself[29]. A direct repressor of Stat92E is Su(var)2-10 / Protein inhibitor of activated STAT (PIAS)[30], a SUMO ligase whose orthologues (PIAS1-4) in mammals SUMOylate and thereby inactivate STAT proteins[31]. We drove two independent *Su(var)2-10* RNAi constructs in glia using *repo-GeneSwitch (repo-GS)* where RNAi expression was induced only in adults to circumvent lethality. It also gave us opportunity to reduce the native Su(var)2-10 level directly before and after injury, thus preventing adverse effects caused by developmental defects. Unexpectedly, *Su(var)2-10* RNAi relieved Stat92E reporter repression predominantly following injury (Fig. 3A-B). This suggests that Su(var)2-10 elimination is required for efficient Stat92E-dependent activation after injury. In contrast to the effect caused by the knockdown or abrogation of an autophagy related component, *Su(var)2-10* depletion enhanced glial Stat92E activity. From this, we can draw the conclusion that autophagy plays an activator role, while Su(var)2-10 inhibits Stat92E. Therefore, we wondered whether Su(var)2-10 relays the repressive effect of autophagy disruption onto Stat92E reporter activation. While knockdown of *Atg16* abrogated *10xStat92E-GFP* activation, depletion of *Su(var)2-10* in this background restored the normal magnitude of Stat92E response to injury (Fig. 3C,D). In contrast, introducing a second inert UAS construct into the context of *Atg16* RNAi did not restore normal activation (Fig. S3A,B). This indicates that Su(var)2-10 can mediate the effect of autophagy on Stat92E-dependent transcription.

**Su(var)2-10 mediates the autophagic modulation of Stat92E activity upon injury by being subject to degradation**

Next, we wanted to validate the hypothesis that Su(var)2-10 autophagic degradation leads to Stat92E activation. We depleted *Atg16* in glia and examined Su(var)2-10 levels in the adult brain following antennal ablation. Removal of antennae results in axon fragmentation in the

antennal lobe (AL) that triggers reactivity in surrounding glia[15]. Su(var)2-10 is mainly nuclear due to its transcriptional repressor and chromatin organizer functions[30,32]. Presumably, higher overall Su(var)2-10 levels result in more nuclear abundance and increased nuclear repressor activity. Therefore, we coexpressed nuclear GFP in glia and examined the co-localizing Su(var)2-10 pool. Su(var)2-10 levels were elevated upon *Atg16* silencing in both uninjured and injured conditions in glia nuclei adjacent to the AL (Fig. 4A-C). We confirmed the specificity of the Su(var)2-10 antibody on Western blots of Su(var)2-10::EGFP ectopically expressed in Schneider 2 R+ (S2R+) *Drosophila* cell culture (Fig. S3C). These results suggest that Su(var)2-10 could be an autophagic cargo and explain repression of Stat92E after injury in *Atg16* deficiency by higher inhibitory Su(var)2-10 levels in the nucleus.

Interestingly, we found that nuclear Su(var)2-10 colocalizes with Atg8a in glia in many cases (Fig. 4D). Although we did not find a consensus LIR motif in Su(var)2-10, the interaction with Atg8a can be mediated by other labels[21]. Su(var)2-10 is known to autoSUMOylate itself[33,34]. We found that SUMO colocalizes with Su(var)2-10+ and Atg8a+ structures inside nuclei (Fig. 4D). However, Su(var)2-10 degradation is supposed to occur in the cytoplasm if it is an autophagy cargo[21]. Accordingly, we also found cytoplasmic structures which were double positive for Su(var)2-10 and Atg8a in glia in the *Drosophila* brain around the antennal lobe (Fig. 4E). Therefore, Su(var)2-10 colocalizes with Atg8a and is likely degraded in the cytoplasm by autophagy.

We also tested Su(var)2-10 degradation in a heterologous system. We transfected S2R+ cells with *Su(var)2-10::EGFP* and treated cells with Bafilomycin A1 (BafA1), a V-ATPase proton pump inhibitor that prevents lysosomal acidification. Su(var)2-10 levels increased upon BafA1 treatment indicating lysosomal degradation of this protein (Fig. 4F,G). Next, we hypothesized that autoSUMOylation of Su(var)2-10 might be a lysosomal degradation signal. The C-terminal domain (CTD) of Su(var)2-10 interacts with SUMO. Mutating two residues in the CTD2 region (*CTD2mut*) disrupts SUMO binding and autoSUMOylation of Su(var)2-10[34]. This leads to a decreased nuclear : cytoplasmic Su(var)2-10 ratio *in vivo*. Using the same *CTD2* mutant construct, we found that baseline levels of CTD2mut are increased relative to the wild-type in S2 cells hinting to a degradation defect (Fig. 4F,G). Interestingly, CTD2mut protein levels were insensitive to BafA1 treatment that suggests that SUMOylation-deficient Su(var)2-10 cannot undergo lysosomal degradation.

Finally, we aimed to reveal whether Su(var)2-10 physically interacts with Atg8a *in vivo*. Atg8a serves as a platform for binding of a selection of autophagy cargos and cargo receptors. After precipitating mCherry::Atg8a from whole fly extracts, we found interaction between certain

Su(var)2-10 isoforms and Atg8a (Fig. 4H). We also identified a Su(var)2-10 band that was specific to the eluate showing that it is enriched in the Atg8a interactome and may constitute a modified version of a lower isoform. Collectively, these results led us conclude that interaction of Su(var)2-10 with Atg8a in the nucleus and in the cytoplasm will trigger its autophagic breakdown possibly via its conjugation to SUMO.

### *vir-1* but not *drpr* is upregulated by autophagy-activated Stat92E in glia following wing transection

What are the relevant targets of this autophagy-regulated Su(var)2-10/Stat92E axis in glial injury responses? It has been shown that following antennal ablation, baseline *drpr* expression in the brain increases via Stat92E-dependent transcription under the control of Drpr signalling, creating a positive feedback loop[16]. This is required for the efficient degradation of the significant amount of debris generated during injury. We decided to monitor *drpr* transcription after injury to see whether it is under the influence of autophagic regulation. We converted a MiMIC insertion in *drpr* (*drpr*$^{MI07659}$) by introducing a *Trojan Gal4* cassette to fully capture the scope of *drpr*-dependent transcription (Fig. S4A). We expressed the recently developed transcriptional reporter *UAS-TransTimer*[35] with *drpr-Gal4.* TransTimer relies on the ratio of destabilised nuclear GFP versus a stable nuclear RFP to monitor dynamic changes in transcription. *drpr-MiMIC-Gal4* flies did not show *TransTimer* upregulation after wing injury (Fig. S4B,C). Next, we asked whether the complexity of *drpr* enhancer regulation in the wing hinders the detection of the increase in *drpr* levels. To this end, we drove *UAS-TransTimer* with an intronic *drpr* enhancer-*Gal4* (*dee7-Gal4*) that harbors a functional Stat92E binding site (Fig. S4A) and has been shown to upregulate transcription after injury[16]. First, we verified that *dee7* is activated in the brain after antennal injury as described previously (Fig. S5A)[16]. Despite this activation, we failed to observe an increase in *dee7-Gal4>TransTimer* flies in the number of RFP puncta 3 days after wing injury (Fig. S5B,C). We conclude that *drpr* upregulation by injury is absent in the wing injury model and it is apparently not a prerequisite for efficient debris processing in the wing nerve.

The JAK-STAT pathway underlies many immune pathways including cytokine signalling and viral defense[36]. We screened immunity-related gene reporters and found that *vir-1-GFP*[37] (Fig. 5A) is robustly upregulated after wing injury (Fig. 5B-E). *vir-1*-produced GFP colocalized with glially driven myr::tdTomato in the wing nerve indicating glial *vir-1* induction (Fig. S6A).

Stat92E signalling- driven *vir-1* is one of the most strongly induced transcripts after viral infection in *Drosophila*[37]. However, besides its supposed systemic antiviral immunity role, *vir-*

*1* has been found to be expressed in glia. *vir-1* is a target of Gcm, a master regulator of glial cell fate[38] and is also a longitudinal glial cell marker in the embryo[39]. Curiously, *vir-1* was described to be markedly upregulated in glia specifically one day after traumatic brain injury but not later[40]. We verified these data by using the *vir-1-GFP* reporter in uninjured and injured fly brains. 1 day post antennal ablation showed a significant increase in the reporter GFP levels in glia in and around the AL (Fig. 5F, G). This alludes to an important role for *vir-1* in glial adaptation to injury.

*vir-1* has seven transcript isoforms. *RE* and *RD* are shorter and encompass only the 3' half of the longer isoforms (*RA, RB, RG*). Therefore, their transcription initiation is offset relative to these longer variants. We found that after wing injury, isoforms *RA* and *RB* are upregulated while *RE* is not (Fig. S6B). This indicates that an injury-responsive enhancer resides in the proximity of the long isoform transcriptional start site.

To corroborate that *vir-1* is a glial Stat92E target, we silenced *stat92e* acutely in adult glia. This abrogated *vir-1-GFP* induction in the wing nerve in response to injury (Fig. 5B,C). This prompted us to investigate whether autophagy impacts *vir-1* expression similar to the *10xStat92E-GFP* reporter. We expressed *Atg16* RNAi in glia and followed *vir-1* induction after injury. While *vir-1* still showed some upregulation upon *Atg16* depletion, this change was not significant when compared to uninjured wings (Fig. 5D,E). Accordingly, we propose that autophagy may modify glial reactive states by acting on this important innate immune locus in glia via Stat92E.

## Discussion

We have uncovered a mechanism of Stat92E transcription factor activation based on autophagy-mediated clearance of a direct repressor. This switch ensures proper glial Stat92E-dependent responses after nerve injury that may contribute to glial reactivity.

The vital role of autophagy in glia biology has just begun to be unravelled[41,42,43]. The aging brain features neuroprotective microglia that show elevated levels of autophagy[44]. Autophagy limits neuroinflammation as it degrades the inflammasome component NLRP3 in microglia to prevent cytokine release and proinflammatory responses[45]. We find that in addition to these roles, autophagy can also positively regulate glial reactivity by impacting a major immune signalling pathway. The autophagic elimination of Su(var)2-10 provides an alternative to canonical JAK-dependent Stat92E regulation that is apparently not employed in glial injury

signalling[16]. LC3-associated phagocytosis is triggered in glia in response to injury via Drpr[26]. We excluded the role of LAP in Stat92E-dependent transcription using LAP-disrupting glial silencing of a crucial LAP effector, *Rubicon* and autophagy-specific genes. How and if injury boosts selective autophagy to remove Su(var)2-10 is an open question. Bulk autophagy in glia, as measured by the *mCherry-GFP-Atg8a* flux reporter, is not elevated upon wing transection. We can see significant increase in Su(var)2-10 levels upon *Atg16* knockdown in glia and in S2 cells both in injured and uninjured conditions. *10xStat92E-GFP* reporter data yield contrasting results since if *Su(var)2-10* is eliminated from glia via silencing, Stat92E activity only increases when flies are simultaneously injured. However, it is not unexpected that Su(var)2-10 removal alone would be insufficient to trigger Stat92E activation. Stat92E activation still depends on tyrosine phosphorylation[16,46] for its proper function in reactive glia. Therefore, we believe that Stat92E operates as a coincidence detector integrating signals from autophagic removal of Su(var)2-10 and activating phosphorylation for full activation.

In support of selective autophagic elimination of Su(var)2-10, we discovered that it is lysosomally degraded, and an autoSUMOylation-defective form of Su(var)2-10 is not subject to this clearance. SUMOylation regulates many developmental and critical cellular processes and enables the quick responsiveness to environmental and homeostatic changes. There is indeed evidence that autophagy could contribute to the elimination of SUMOylated Ataxin-3[47]. Ubiquitylation of SUMOylated proteins by SUMO-targeted ubiquitin ligases (STUbLs) can lead to subsequent degradation[48,49]. We detected Su(var)2-10 colocalization with Atg8a in the cytoplasm in brain glia. Nuclear Su(var)2-10 also colocalizes with both SUMO and Atg8a. Given that the colocalizing structures are larger than single molecules and vesicles are excluded from the nucleus, these are likely liquid-liquid phase-separated (LLPS) multimolecular aggregates. SUMOylation regulates stress granule assembly[50] and other types of phase separation[51], and the Su(var)2-10 ortholog PIAS1 is predicted to undergo LLPS[52]. The lack of a LIR motif suggests that Su(var)2-10 does not interact directly with Atg8a but requires labelling, perhaps by Ub family proteins, for elimination by autophagy. Stat92E activation defects in the *Atg8a*$^{LDS}$ mutant, SUMO-dependent lysosomal degradation of Su(var)2-10 and its colocalization and interaction with Atg8a all point to selective autophagic clearance of Su(var)2-10.

We make the surprising finding that *vir-1*, a supposed antiviral molecule [37], is strongly induced in glia after axon injury by Stat92E both in wing and CNS. In a recent study, it was also shown that *vir-1* is strongly upregulated in glia similarly to other antimicrobial peptides after closed head traumatic brain injury[40]. *vir-1* expression may be differentially regulated among glial

classes since *vir-1* expression defines a distinct subset of plasmatocytes[53]. *vir-1-GFP* is induced in ensheathing glia and possibly astrocytes in the brain after injury (Fig. 5F). The cellular role of Vir-1 is not known. However, it appears that Vir-1 features a signal peptide and in fact localizes to the extracellular space in the foregut[54]. Therefore, we hypothesize that it can perform signalling or antimicrobial functions.

*drpr* upregulation after injury has been shown to be an adaptive response for enhanced debris phagocytosis[55]. We find that *drpr* is highly expressed in wing nerve glia in uninjured conditions and it is not induced further by wing transection. This would indicate high phagocytic activity in wing glia, however, axon debris clearance takes substantially longer in the wing as compared to antennal lobe glomeruli in the brain[15,56]. Therefore, we propose that Drpr levels do not readily predict phagocytic capacity in glia.

Glial reactivity is expected to rely heavily on Stat92E signalling. Phosphorylated Stat3 serves as a marker for reactive astrocytes in mice[57]. Stat3-dependent transcription counteracts traumatic brain injury, motor neuron injury, spinal cord injury and neonatal white matter injury, however, it contributes to degeneration in AD models[57]. Glial Stat92E activation is also observed in an amyloid-beta overproducing *Drosophila* model[58]. Accordingly, autophagy activation may promote Stat92E signalling and thereby assist functional recovery after injury. In line with this, autophagy deficiency in microglia predisposes to more neurodegeneration and demyelination in a multiple sclerosis (MS) model[44]. Based on our findings, we expect that the benefits of autophagy stimulation in the nervous system will partly be manifested through STAT family-driven glial reactivity.

## Figure legends

**Figure 1. *Atg16* is required for Stat92E-, but not for AP-1-dependent transcription during progression of glial reactivity**

(A,B) Single-slice images showing the effect of *Atg16* and control firefly luciferase (*luc*) knockdown in glia on the *10xStat92E-GFP* and *TRE-GFP* reporters in uninjured and injured wing nerves at 3 dpi. RNAi expression was induced by *repo-Gal4*. Arrows point to glial reporter expression, while arrowheads denote the epithelial GFP surrounding the veins. Scale bar: 5 µm. (C) Quantitative analysis of the activity of the reporter constructs (A,B) based on normalized GFP intensity. Unpaired, two-tailed Mann-Whitney test was applied in each comparison. Truncated violin plots are shown with median and quartiles. **** $p < 0.0001$, *** $p = 0.0004$, ns = 0.0743. n = 13, 17, 13, 16, 18, 16, 16, 17. (D) Single-slice images of wing nerves showing

10xStat92E-GFP signal 3 dpi in *Atg8a*$^{null}$ and *Atg5*$^{5cc5}$mutant backgrounds. The effect caused by the *Atg5*$^{5cc5}$ mutation can be rescued by introducing the *Atg5::3xHA,* a promoter-driven *Atg5* transgene. Arrows point to glia, while arrowheads mark the epithelium. Scale bar: 5 µm. (E,F) Quantitative analysis of *10xStat92E-GFP* activation based on normalized GFP intensity. Truncated violin plots are shown with median and quartiles. Unpaired, two-tailed *t*-test (*w*$^{1118}$*(E), Atg5*$^{5cc5}$*::3xHA*) and unpaired, two-tailed Mann–Whitney test (*w*$^{1118}$*(F), Atg8a*$^{\Delta 12}$*, Atg5*$^{5cc5}$) were used for statistics. **** $p < 0.0001$, *** $p = 0.0002$, ns (E) > 0.9999, ns (F) = 0.1179. n (E) = 10, 13, 4, 6. n (F) = 17, 18, 11, 12, 11, 14.

**Figure 2. Selective autophagy but not LAP drives Stat92E-dependent transcription in injury signalling**

(A,B) Single-slice images of wing nerves showing 10xStat92E-GFP signal in different glial RNAi backgrounds. *Atg13* is required only for autophagy, while *Rubicon* is indispensable for LAP. RNAi expression was induced by *repo-Gal4*. Arrows point to glial GFP, while arrowheads denote the epithelial GFP signal. Scale bar: 5 µm. (C,D) Quantitative analysis of *10xStat92E-GFP* activation (A, B) based on normalized GFP intensity. Truncated violin plots are shown with median and quartiles. Unpaired, two-tailed Mann–Whitney test was used for statistics. *** p(C) = 0.0002, *** p(D) = 0.0004, ** p = 0.0021, ns = 0.9195. n (C) = 10, 9, 18, 20. n (D)= 19, 19, 18, 18. (E) Single optical slices showing the effect *of Atg8a*$^{LDS}$ mutation on *10xStat92E-GFP* activation. *Atg8a*$^{LDS}$ has a mutation in its LIR motif docking site thus specifically abrogates selective autophagy. Arrows point to glial GFP signal, while arrowheads denote the epithelial GFP. Scale bar: 5 µm. (F) Quantitative analysis of *10xStat92E-GFP* activity (C,D) based on normalized GFP intensity. Truncated violin plots are shown with median and quartiles. Unpaired, two-tailed Mann-Whitney test was used for each comparison. ** p = 0.0053, ns = 0.7789. n = 9, 16, 8, 7.

**Figure 3. Su(var)2-10 is a Stat92E repressor in glia and mediates the autophagic modulation of Stat92E activity upon injury**

(A) Single optical slices showing the disinhibition effect of two independent *Su(var)2-10* RNAi constructs on Stat92E activity (*10xSTAT92E-GFP*) using the *repo-GS* system in glia. RNAi expression was induced by RU486 for 5-7 days after eclosion prior to injury and lasted for the duration of the experiment. Arrows point to glial GFP, while arrowheads denote the epithelial GFP signal. Scale bar: 5 µm. (B,C) Quantitative analysis of normalized 10xStat92E-GFP signal

shown in (A). Unpaired, two-tailed Mann-Whitney test was used for pairwise comparisons. Truncated violin plots are shown with median and quartiles. *** p = 0.0002, * p (B) = 0.0120, * p (C) = 0.0482, ns = 0.4742. n (B) = 13, 13, 15, 16. n (C) = 21, 14, 26, 18. (D) Epistatic interaction between *Su(var)2-10* and *Atg16*. Single-slice images of wing nerves showing 10xStat92E-GFP signal upon glial RNAi. RNAi expression was induced by RU486 for 5-7 days after eclosion prior to injury and lasted for the duration of the experiment. *Atg16* silencing impairs the activation of Stat92E after injury that is restored by simultaneous *Atg16* RNAi and *Su(var)2-10* knockdown. Arrows point to glial GFP, while arrowheads denote the epithelial GFP. Scale bar: 5 µm. (E) Quantitative analysis of normalized 10xStat92E-GFP signal shown in (D). Truncated violin plots are shown with median and quartiles. Unpaired two-tailed Mann–Whitney test was used for all comparisons. **** p < 0.0001, * p (*luc*) = 0.0124, * p (*Atg16 + 29448*) = 0.0127, ns = 0.2939. n = 15, 19, 14, 16, 16, 18, 10, 11.

**Figure 4. Su(var)2-10 in glia is subject to autophagic degradation**

(A) Single optical slices showing Su(var)2-10 abundance in brain glia around the AL in glial *luc* and *Atg16* KD background without injury and 1 day after antennal ablation. Su(var)2-10 is predominantly nuclear. Glial nuclei are labelled by *repo-Gal4>NLS-GFP.* Arrows denote glial nuclei. Note the accumulation of Su(var)2-10 in glia versus neuron nuclei, and that a fraction of NLS-GFP is also retained in the cytoplasm. Scale bars: 20 µm and 5 µm. (B,C) Quantitative analysis of Su(var)2-10 nuclear intensity normalized to background signal in single optical slices shown in (A). Truncated violin plots are shown with median and quartiles. Unpaired, two-tailed Mann–Whitney test was used for statistics. **** p < 0.0001, ** p = 0.0033. n (B) = 109, 90. n (C) = 80, 64. (D) Single optical slices taken of the brain around the two antennal lobes, shown in four different channels. Magnified images of the nuclei of interest are shown below. Arrowheads point to the glial nuclei of interest, while arrows denote the exact location of the colocaliziation. Nuclei are stained with DAPI, native *mApple::Atg8a* expression is driven in glia by *repo-Gal4*, without further staining, combined with anti-Su(var)2-10 and anti-SUMO immunostaining. Su(var)2-10 - SUMO - Atg8a colocalization can be seen in more glial nuclei. Scale bar for brain images: 10 µm, scale bar for nucleus images: 2 µm. (E) Confocal single-slice, multi-channel images, showing Su(var)2-10 - Atg8a colocalization outside the nuclei, in glial cytoplasm. Magnified images of the areas outlined by the rectangles can be seen below. Arrows point to the exact location of the colocalization. Nuclei are stained with DAPI, *mApple::Atg8a* expression is driven in glia by *repo-Gal4*, and the signal is amplified by anti-mCherry staining, while Su(var)2-10 is stained with anti-Su(var)2-10. Scale bar for brain

images: 10 µm, scale bar for nucleus images: 2 µm. (F) S2 cells transiently expressing wild-type and autoSUMOylation defective CTD2 mutant Su(var)2-10::EGFP were treated with Bafilomycin A1 (BafA1) for 4 hours, and total Su(var)2-10 levels were assessed by anti-GFP Western blot. Anti-α-tubulin serves as a loading control. (G) Quantification of Su(var)2-10 abundance normalized to α-tubulin as in (F). Shown is the mean and standard deviation, one-way ANOVA with Holm- Šídák test for multiple comparison correction was used for statistics. n = 4, 3, 4, 4. (H) Co-immunoprecipitation of Su(var)2-10 with mCherry::Atg8a. RFP-s from *daughterless* (*da*)-*Gal4*-driven myr::tdTomato (Tomato) and mCherry::Atg8a (Ch::Atg8a) whole adult fly extracts were precipitated with RFPTrap beads. myr::tdTomato serves as a negative control. Eluates are shown on the right, crude extract inputs (10 ug) on the left. The double band in mCherry::Atg8a corresponds to the lipidated and unlipidated forms. Orange arrow indicates an eluate-specific Su(var)2-10 species. Western blots were revealed by anti-mCherry and anti-Su(var)2-10.

**Figure 5. *vir-1* expression is regulated by Stat92E and is subject to autophagic control in glia after wing injury**

(A) Schematic representation of *vir-1-GFP* reporter construct: 2.6kb of *vir-1* upstream sequences drive GFP expression[37]. The *vir-1* fragment includes the first intron and the first exon. (B) Stat92E-dependent activation of glial *vir-1-GFP* after axonal injury. Single-slice images of wing nerves showing vir-1-GFP signal upon glial *stat92E* RNAi. RNAi expression was induced by RU486 for 5-7 days after eclosion prior to injury and lasted for the duration of the experiment. Arrows point to glial reporter expression, while arrowheads denote the epithelium. Scale bar: 5 µm. (D) *vir-1-GFP* induction upon injury in *Atg16* knockdown flies. Single-slice images of wing nerves showing vir-1-GFP signal upon glial *Atg16* RNAi. RNAi expression was induced by RU486 for 5-7 days after eclosion prior to injury and lasted for the duration of the experiment. Arrows point to glial GFP, while arrowheads denote the epithelial GFP signal. Scale bar: 5 µm. (C,E) Quantification of vir-1-GFP signal shown in (B) and (D). Truncated violin plots are shown with median and quartiles. Unpaired, two-tailed Mann–Whitney test was used for each pairwise comparison. **** $p < 0.0001$, ns (C) = 0.0512, ns (E) = 0.1201. n (C) = 16, 19, 12, 11. n (E) = 11, 13, 11, 14. (F) *vir-1* induction in brain by injury. Single-slice optical images obtained by a confocal miscroscope showing vir-1-GFP signal around the AL, without and 1 day after antennal ablation. Scale bar: 20 um. (G) Quantitative analysis of normalized GFP signal in brain shown in (F). Truncated violin plots with median

and quartiles. Data were quantified by using unpaired, two-tailed Mann–Whitney test. **** $p < 0.0001$. n = 12, 12.

**Fig. 6. Schematic illustration of the autophagy-regulated Su(var)2-10/Stat92E axis in glia after neural injury**

Upon neural injury, glial Stat92E becomes activated by simultaneous phosphorylation and derepression. Sufficiently low levels of Su(var)2-10 are continuously maintained by selective autophagy through Atg8a binding - presumably mediated by SUMO -, while phosphorylation occurs in response to injury. Activated Stat92E translocates to the nucleus and binds to Stat92E binding motifs on the regulatory region of genes that are upregulated after axon injury, such as *vir-1*.

## Acknowledgements


Funding

This research was supported by:

- the Momentum/Lendület Grant of Hungarian Academy of Sciences (LP2023-6) (GJ)
- the Young Researchers' Excellence Programme of the National Research, Development and Innovation Office (NRDIO) (FK132183) (AS)
- the Janos Bolyai Research Scholarship of the Hungarian Academy of Sciences (BO/00078/18) (AS)
- the NRDIO New National Excellence Programme (ÚNKP-20-5, ÚNKP-19-4, ÚNKP-18-4) (AS)
- the NRDIO grant KKP129797 (GJ)
- the NRDIO grant PD145868 (AJ)
- the NRDIO grant GINOP-2.3.2-15-2016-00032 (GJ)
- and the Biotechnology National Laboratory program of the National Research, Development and Innovation Office (NKFIH-871-3/2020) (GJ).
- the National Talent Programme - Scholarship for the Young Talents of the Nation (NTP-NFTÖ-22-B-0055) (VV),
- the New National Excellence Programme (ÚNKP-23-3 -SZTE-537) (VV)

- and the National Academy of Scientist Education Program of the National Biomedical Foundation under the sponsorship of the Hungarian Ministry of Culture and Innovation (ZE, AS and GJ).

We would like to give a special thanks to László Tirián and Julius Brennecke for the mouse anti-Su(var)2-10 antibody, Giacomo Cavalli for the rabbit anti-SUMO antibody, Marc Freeman for the *dee7-Gal4* and other stocks, Jean-Luc Imler for the *vir-1-GFP,* Melinda Bence and Miklós Erdélyi for *Su(var)2-10* RNAi stocks and further support, Zoltán Hegedűs from the Laboratory of Bioinformatics for bioinformatic analyses, the Bloomington Stock Center and the Vienna *Drosophila* Resource Center for the ordered fly stocks, the Developmental Studies Hybridoma Bank for antibodies, Szilvia Bozsó and Ildikó Kresákné Erdődi for technical assistance. We also acknowledge the provided microscopy support of the Cellular Imaging Laboratory (HUN-REN Biological Research Centre). We are grateful to Gábor Csordás, Arindam Bhattacherjee, András Blastyák and Tamás Maruzs for fruitful discussions. Fig. 5A, 6, S1A and S2A were created by BioRender.com.

## Author contributions

Conceptualization: V.V., A.S. and G.J.; Investigation: A.S., V.V., Z.E., E.F.J., A.S.C., A.J., M.C., D.F.B., A.R.G. and G.J. Resources: A.J., Z.E., D.F.B., A. R. G.; Results interpretation: A.S., V.V., Z.E., E.F.J., A.S.C., A.J., M.C., D.F.B., A.R.G. and G.J. Writing: V.V., Z.E., A.S. and G.J.; Manuscript revision: V.V., Z.E., A.S., A.S.C., and G.J.; Supervision: A.S. and G.J.; Funding acquisition: A.S. and G.J.

## Competing interests

The authors declare no competing interests.

## Data availability

All data needed to evaluate the conclusions in this paper are present in the paper and its Supplementary Information. Other data associated with the article such as raw data are available upon request.

## Materials availability

All materials, *Drosophila* stocks and related information are available from the corresponding authors upon reasonable request.

## Ethics statement

The research presented here uses the species *Drosophila melanogaster* for which no ethical approval is required in the HUN-REN Biological Research Center, Institute of Genetics or by Hungarian authorities. Maintenance of transgenic *Drosophila* melanogaster at the Institute is regulated by license No. SF/66/2014 of the Gene Technology Authority Registry, Ministry of Agriculture of the Hungarian Government.

## Materials and methods

### *Drosophila* stocks and maintenance

The flies were kept at 25°C on a medium containing cornmeal, yeast, agar and dextrose with Nipagin as a preservative in reusable glass vials and bottles. For our experiments, we injured male *Drosophila melanogaster* that were 2–7 days old after eclosion. During our experiments, we favored male flies to avoid technical inconvenience related to egg laying and to prevent larvae from making the medium too liquid and sticky. The animals were anesthetized by carbon dioxide. Progeny of *repo-GS* crossed with RNAi lines were raised on normal food during development, then males were kept for 5-7 days on food supplemented with 25 µg/ml RU486/mifepristone (Acros Organics) before axotomy and thereafter during the course of the experiment. Injury was carried out on 7-12 day old flies. The supplemented medium used for experiments using *vir-1-GFP* contained 125 µg/ml RU486.

The following stocks were ordered from Bloomington *Drosophila* Center: *repo-Gal4 (7415),* $w^{1118}$, *daughterless-Gal4 (95282)*, *vasa>Cas9* (*51323*), *TRE-EGFP (59010), firefly luciferase*$^{JF01355}$, *Atg8a*$^{TKO.GS04635}$ (*80828*), *Su(var)2-10*$^{JF03384}$ *(29448), Su(var)2-10*$^{HMS00750}$ *(32956), UASp-mCherry::Atg8a (37750), UASp-GFP-mCherry-Atg8a (37749), UAS-TransTimer (93411), drpr*$^{MI07659}$ *(843909), UAS-2xEYFP (60291), vas-int, w[*], hs-Cre (60299), pP{lox(Trojan-GAL4)x3} (60310)*[59], *stat92E*$^{GL00437}$, *10XStat92E-EGFP (26197), UAS-NLS::GFP (4775) and 10XUAS-IVS-myr::tdTomato (32221).*

The following stocks were sent by Vienna *Drosophila* Resource Center: *Rubicon*$^{KK108247}$, *Atg13*$^{KK100340}$, *Atg16*$^{KK10232}$ and *ref(2)P*$^{KK105338}$. The *Atg5*$^{5cc5}$ [60], *Atg8a*$^{LDS}$ [27], *Atg5*$^{5cc5}$*; Atg5::3xHA* [24] stocks were formerly created and published. We generated the *10xStat92E-GFP/CyO; repo-Gal4/Tm6, TRE-GFP/CyO; repo-Gal4/Tm6, NLS-GFP/CyO; repo-Gal4/Tm6, vir-1-GFP/CyO; repo-GS/Tm6* by standard crossing schemes. The following stocks received as gifts were much appreciated: *repo-GeneSwitch* was kindly shared by Véronique Monnier (Université de Paris, BFA Unit of Functional and Adaptative Biology, UMR 8251, France). *dee7-Gal4* (*drpr* enhancer-Gal4) was kindly sent by Marc Freeman (Vollum Institute, Oregon Health & Science University, USA) and *vir-1-GFP.2.6 (vir-1-GFP)* by Jean-Luc Imler (IBMC, University of Strasbourg, France).

The *Atg8a*$^{null}$ frameshift mutant was generated by CRISPR-Cas9 editing. To generate this null allele (*Atg8a*$^{\Delta 12}$), we used the *Atg8a*$^{TKO.GS04635}$ gRNA line and crossed it with *vasa>Cas9* transgenic flies. We screened candidate mutant lines by PCR and Sanger sequencing and identified the *Atg8a*$^{\Delta 12}$ allele that carries an 8 bp deletion based on sequencing data (Fig. S2A), which deletion causes frameshift in all isoforms of the Atg8a gene.

The 2xmApple::Atg8a construct was cloned into the pACU vector (Addgene #58373). mApple sequences were amplified from the pCDH-TMEM106b-mApple vector (Addgene #179385). The PCR products which were used for the construct assembly with the NEBuilder® HiFi DNA Assembly Master Mix (New England Biolabs) are listed in the Supplementary Table. We validated the constructs by Sanger sequencing and we were able to detect mApple fluorescence in induced transfected S2 cells cotransfected with pMTGal4. The transgenic *Drosophila* line was established by the *Drosophila* Injection Service in the Biological Research Center, Szeged (Hungary). The transgene was inserted into the *attP40* (2L) landing site.

A MiMIC transgene (*MI07659*) located in intron 6 of *drpr* was converted into a *drpr-Gal4* fusion gene using a *Gal4* donor, so that Gal4 is produced instead of most of the *drpr* coding sequence. We followed the protocol described in Diao et al. 2015[59] by crossing in recombinase and donor transgenes. A donor cassette containing a splice acceptor (*SA*), the *Gal4* to be encoded in the correct frame and finally a stop codon and polyadenylation site between two *attB* sites was mobilized and circularized by heat shock-inducible Cre. Integration into *MI07659* was achieved by vas-dΦC31. Candidate progeny were screened for *drpr* expression by crossing to *UAS-2xEYFP*. Integration into *drpr* was validated by PCR. *drpr-Gal4* is expressed in glia in the CNS and PNS in addition to other tissues.

**Rearing stocks with low bacterial content for RT-qPCR**

We placed approximately 100 animals from the used strains into a cylinder containing black egg-laying agar coated with yeast for one night. Embryos were dechorionated in 4-5% hypochlorite on a filter for 1 minute followed by washing with flowing distilled water. Finally, we removed the filter fabric, placed it on a paper towel, and transferred the eggs into new vials containing a nutrient medium mixed with antibiotics already described[61]. We aimed at creating a fly flood that would partially kill the *Drosophila* microbiome to prevent the contamination coming from bacteria during the RNA purification. First, we autoclaved the commonly used cornmeal-yeast-agar-dextrose–Nipagin medium. Then, we mixed the food with 0.25 mg/ml ampicillin, tetracycline, streptomycin, and 1 mg/ml kanamycin[61]. Flies were kept for at least 3 generations on antibiotics. The concentration of the antibiotics were reduced to half 20 days before the sample collection to increase the amount of progeny. The food cocktail preparation and fly transfer took place in a laminar box using only autoclaved and sterile tools.

**Wing injury**

In all experiments we carried out in *Drosophila,* male flies were used. In the wing injury assay, we used the axotomy model developed by Fang et al.[22] and Neukomm et al[23]. In accordance with the model (S1A), we removed half of the wing of flies from the distal end with a straight cut across using microsurgical scissors. For each individual, we only cut one wing, leaving the other intact as an uninjured control. The injured animals were then kept in vials at 25 °C. Three

days after the injury (3 dpi), a strong 10xStat92E-GFP signal was already observable (Fig. S1D,E).

**Antennal ablation**

The antennae were ablated 1 day prior to brain dissection by pulling on with a forceps[15], and the injured flies were kept in vials at 25°C.

**Imaging**

While imaging the reporter signals in the the wing, we focused on a specific region inside the L1 vein. L1 vein curves from the wing margin towards the inner area of the wing, containing axons and glial cells. We analyzed the samples at room temperature (RT) using the Axio Imager.M2 microscope (Zeiss) and the ORCAFlash4.0LT CMOS camera (Hamamatsu) using a Zeiss PlanApochromat 63x/1.40 NA objective. Optical slices were created with a Zeiss ApoTome.2 device which was connected to the microscope. The illumination was provided by the CoolLED pE-4000 system. We captured the images using the Zeiss Zen program.

For measuring the Su(var)2-10 signal in Su(var)2-10 and NLS-GFP co-immunostained brains, the Visitron VisiScope Spinning Disk Confocal Microscope (Visitron Systems GmbH, Puchheim, Germany) was used. The optical slices were created with an Olympus LUCPlanFl 40x NA 0.60 objective for quantification, while magnified images shown in the article were captured with an Olympus PlanApo 60x NA 1.42 (oil) objective. Detection was based on an Andor Zyla 4.2 PLUS camera.

For the three channel fluorescence images 405 nm excitation with 405/488/561 tri band emission filter, 488 nm excitation with 525/50 emission filter, and 561 nm excitation with 605/70 emission filter were used with a triple band 405/488/561 dichroic mirror. For the four channel fluorescence images 405 nm excitation with 405/488/561 tri band emission filter, 488 nm excitation with 525/50 emission filter, 561 nm excitation with 605/70 emission filter, and 640 nm excitation with 700/75 emission filter were used with a quad band 405/488/561/640 dichroic mirror. Channels were acquired in sequential mode, after the performed Z sectioning. We used a disk with 50 um pinholes.

For vir-1-GFP signal detection in brain, we used an LSM800 (Zeiss) inverted laser scanning confocal microscope. The brains were imaged at RT with a Zeiss Plan-Apochromat 40x/1.3 NA oil immersion objective with a Z-step of 2.00 µm.

The same microscope settings (illumination, exposure time, laser intensity) were used for all conditions and genotypes within one experiment.

**Immunostaining of adult brains**

Immunostaining of adult brains was performed as described with some modifications[62]. Adult brains were dissected from living flies in ice-cold phosphate buffered saline (PBS) and placed immediately in 4% paraformaldehyde in PBS with 0.3% Triton X-100 (PBT) on ice. Brains were fixed for 1 h at 25 °C. After two quick rinses with PBT, brains were washed three times 20 min each. Following blocking in 5% fetal bovine serum (FBS) in PBT for 1 h at RT (RT), brains were incubated with the primary antibody (mouse anti-Su(var)2-10[63] 1:100, rabbit anti-GFP 1:1000 Thermo Fisher Scientific A-11122, rabbit anti-SUMO[64] 1:200, rabbit anti-mCherry NBP2-25157, Novis Biologicals 1:500) for 3 days at 4 °C in 5% FBS in PBT. The SUMO antibody was gently provided by Giacomo Cavalli (Institute of Human Genetics (IGH), Montpellier, France) and the Su(var)2-10 antibody by Julius Brennecke (IMBA, Vienna, Austria). Washes were done as before and brains were incubated with the fluorescently labelled secondary antibody (goat anti-rabbit Alexa Fluor 488, A-11034, goat anti-mouse Alexa Fluor 568, A-11031, from Thermo Fisher Scientific, all 1:1000 diluted) in 5% FBS in PBT 2 days at 4 °C in darkness. The secondary antibody was removed by two quick rinses, and DAPI (1:15000) was put into the following first wash with PBT. Brains were washed three times 20 min each. After the washes, the brains were mounted in Vectashield (Vector Laboratories, H-1000-10), and the samples were kept in darkness at 4°C until imaging.

**RNA purification and RT-qPCR**

For RNA isolation, we collected around 150-200 wings per sample using only autoclaved tools with autoclaved wiping papers placed on the fly sorting pad previously washed with 70% ethanol. The wings were swept in TRI Reagent (Zymo Research)-containing microcentrifuge tubes, using a funnel. We homogenized the samples directly after putting them into TRI Reagent. Total RNA was purified with the Direct-zol RNA Microprep (Zymo Research). DNAse I digestion was also applied. 76 ng total RNA was reverse transcribed in 20 µl reaction volume with the RevertAid First Strand cDNA Synthesis Kit (Thermo Scientific). qRT-PCR was performed in 20 µl reactions in technical triplicates using the PerfeCTa SYBR Green FastMix (Quantabio) with 0.5 µl cDNA and cycled on a Rotor-Gene Q qPCR machine (Qiagen) running Rotor-Gene software 2.3.1.49 (Qiagen), with the following program: 95 °C, 3 min; 45 cycles of 95 °C, 20 s, 60 °C, 20 s and 72 °C, 20 s followed by melting curve analysis. The ΔΔCt

method was employed to normalize the data, with *Ribosomal protein L32* (*RpL32*, also known as *rp49*) serving as the internal control. All primers were designed with Primer-BLAST (https://www.ncbi.nlm.nih.gov/tools/primer-blast) with amplicon length set to 70–150 bp. The used melting temperature was 60 °C. One primer spanned an exon-exon junction in all cases. Primers used for RT-qPCR are listed in the Supplementary Table. We normalized the qPCR datasets to RpL32. The ΔCt-derived expression values were adjusted by a common scaling factor to ensure that the average of control values equaled 1 or 100.

### ***Drosophila*** **S2R+ cell culture**

*Drosophila* S2R + cells were cultured in 1x Schneider's *Drosophila* media (GIBCO) supplemented with 10 % fetal bovine serum (GIBCO), penicillin-streptomycin solution (HyClone) in 25-$cm^2$ T-flasks (Thermo Fisher Scientific) at RT. The cells (~$8x10^5$) were seeded in a six well-culture plate and 24 h later were transiently co-transfected with *pUASp-Su(var)2-10-WT::GFP, pUASp-Su(var)2-10-CTD2mut::GFP* and *pMT-Gal4* using the MirusIT-Insect transfection reagent based on the manufacturer's recommendations. S2R+ cells were transfected with 2500 ng of each plasmid. Twenty-four hours after transfection, 0.5 mM of $CuSO_4$ was added to the cells to induce Gal4 expression from the metallothionein promoter. 24h after induction, cells were treated with 100 nM bafilomycin A1 (Invitrogen), and incubated for 4 h. Cell pellets were stored at -80 °C.

### **Immunoprecipitation**

Extracts were prepared from 0.5 ml of 3-7 days old whole flies from *da-Gal4>UAS-myr-tdTomato* and *da-Gal4>UAS-mCherry::Atg8a* genotypes. Flies were homogenized in 0.5 ml extraction buffer (50 mM Tris pH = 7.4, 150 mM NaCl, 2 mM EDTA, 0.5% Nonidet P-40, 5% glycerol, Pierce Protease Inhibitor Tablet (Thermo Fisher Scientific) and Halt Protease and Phosphatase Inhibitor Cocktail (Thermo Fisher Scientific) on ice in a Potter homogenizer. Following centrifugation (15000 g, 15 min, 4 °C), the protein concentration in the supernatant was measured with Pierce Bradford Plus reagent (Thermo Fisher Scientific). 5 mg extract was precleared by rotating with 50 µl of Dynabeads M-280 Streptavidin (Thermo Fisher Scientific) for 1h at 4 °C to absorb bead-binding nonspecific proteins and immuoprecipitated using 50 µl of RFP-Trap magnetic Agarose (ChromoTek) for another 1h at 4 °C. Subsequently, beads were washed with extraction buffer 3 times for 10 min each. Beads were eluted in 20 µl of 2x

Laemmli sample buffer without DTT for 5 min at 100 °C and diluted and supplemented with DTT. Half of the eluted sample was loaded on gels.

**Western blotting**

S2 cell pellets were lysed on ice for 30 min in three times packed volume RIPA buffer (50 mM Tris pH = 8, 150 mM NaCl, 1% Nonidet P-40, 0.5% sodium deoxycholate, 0.1% SDS, Pierce Protease Inhibitor Tablet (Thermo Fisher Scientific), Halt Protease and Phosphatase Inhibitor Cocktail (Thermo Fisher Scientific)) and cleared by centrifugation at 4 C. Protein concentration in the supernatant was measured with Pierce Bradford Plus reagent (Thermo Fisher Scientific). 5 µg total protein was loaded onto 8% polyacrylamide gels. After overnight blotting on Immobilon®-FL PVDF Transfer Membrane. Membranes were blocked with Intercept (TBS) Blocking Buffer (LI-COR) for 1 h at RT. The following primary antibodies were used: rabbit anti-GFP (Thermo Fisher Scientific A-11122), rabbit anti-mCherry (NBP2-25157, Novis Biologicals), mouse anti-Su(var)2-10[63], mouse anti-α-tubulin (Developmental Studies Hybridoma Bank AA4.3) all 1:1000, diluted in Blocking Buffer and incubated for 1 h at RT. Secondary antibodies were the following: anti-mouse IRDye 800CW (926-32210, LI-COR) and anti-rabbit IRDye 680RD (926-68071, LI-COR) 1:15,000, diluted in Blocking Buffer supplemented with 0.02% SDS and 0.2% Tween-20 and incubated for 1h at RT. Dried blots were imaged and quantified in an Odyssey Clx instrument (LI-COR).

**Image analysis**

The signal intensity coming from the fluorescent images were quantified with Fiji (ImageJ 2.9.0, v1.54h). For assessing TRE-EGFP, 10xStat92E-GFP and vir-1-GFP intensity levels in wings, we measured a 174 x 54 px area in each case. When quantifying the intensity of the vir-1-GFP signal in the brain, intensity data were generated from both optic lobes within a 225 x 37 px area. To determine the level of Su(var)2-10 within the nuclei, we randomly selected 10 glial cells marked by *repo-Gal4 > NLS-GFP* from each brain around the AL (except in cases where fewer cells were found). The nuclei were outlined using freehand selection. To measure *drpr* activity in the wing by using *drpr-Gal4 > UAS-TransTimer* flies, we selected an area of 800 x 200 px and measured all the nuclei intensities inside the rectangles. The nuclei were outlined by freehand selection. In *dee7-Gal4 > UAS-TransTimer* brains, we used a 1300 x 1300 px area to count red puncta. In *dee7-Gal4 > UAS-TransTimer* wings, a 600 x 140 px sized

rectangular area was selected for counting red puncta. All fluorescent signals detected in the area of interest were normalized to the background with identical area sizes. Western blot bands were quantified by the Image Studio 5.2 software (LI-COR). Su(var)2-10 signals were normalized to α-tubulin levels.

**Statistical analysis**

Experiments were independently repeated at least two times with different distinctive biological samples, with similar results. The quantified results are represented by truncated violin plots with median and quartiles containing all data points; no data were excluded. The statistical analyses were performed with GraphPad Prism 8.0.1 and 10. We first checked the normal distribution within each data group running the Shapiro-Wilk normality test ($\alpha = 0.05$). Based on these results, we selected the appropriate statistical test to determine the difference between two datasets. When conducting pairwise comparisons on normally distributed data, we performed unpaired, two-tailed Student's *t*-test, while for non-normally distributed data, the unpaired, two-tailed Mann-Whitney test was applied. For the comparison of multiple datasets of normal distribution, one-way ANOVA with Holm- Šídák test for multiple comparison correction was used as in Fig. 4G. No power calculations were performed. For the experiments, we always used a sample size that gave reproducible results, similarly to a relevant article[11], except for Western blot data where n = 3 or 4.

## References


1. Zengeler, K. E. & Lukens, J. R. Microglia pack a toolbox for life. *Trends Immunol.* **45**, 338–345 (2024).

2. Younger, D., Murugan, M., Rao, K. V. R., Wu, L.-J. & Chandra, N. Microglia Receptors in Animal Models of Traumatic Brain Injury. *Mol. Neurobiol.* **56**, 5202–5228 (2019).

3. Balak, C. D., Han, C. Z. & Glass, C. K. Deciphering microglia phenotypes in health and disease. *Curr. Opin. Genet. Dev.* **84**, 102146 (2024).

4. Dominguez, E., Rivat, C., Pommier, B., Mauborgne, A. & Pohl, M. JAK/STAT3 pathway is activated in spinal cord microglia after peripheral nerve injury and contributes to neuropathic pain development in rat. *J. Neurochem.* **107**, 50–60 (2008).

5. Herrmann, J. E. *et al.* STAT3 is a Critical Regulator of Astrogliosis and Scar Formation after Spinal Cord Injury. *J. Neurosci.* **28**, 7231–7243 (2008).

6. Zamanian, J. L. *et al.* Genomic Analysis of Reactive Astrogliosis. *J. Neurosci.* **32**, 6391–6410 (2012).

7. Zhao, J., Zhang, Y., Li, G., Su, X. & Hang, C. Activation of JAK2/STAT pathway in cerebral cortex after experimental traumatic brain injury of rats. *Neurosci. Lett.* **498**, 147–152 (2011).

8. Yan, Z., Gibson, S. A., Buckley, J. A., Qin, H. & Benveniste, E. N. Role of the JAK/STAT signaling pathway in regulation of innate immunity in neuroinflammatory diseases. *Clin. Immunol.* **189**, 4–13 (2018).

9. Jain, M. *et al.* Role of JAK/STAT in the Neuroinflammation and its Association with Neurological Disorders. *Ann. Neurosci.* **28**, 191–200 (2021).

10. Roy, E. R. *et al.* Type I interferon response drives neuroinflammation and synapse loss in Alzheimer disease. *J. Clin. Investig.* **130**, 1912–1930 (2020).

11. Lu, T.-Y. *et al.* Axon degeneration induces glial responses through Draper-TRAF4-JNK signalling. *Nat Commun* **8**, 14355 (2017).

12. MacDonald, J. M., Doherty, J., Hackett, R. & Freeman, M. R. The c-Jun kinase signaling cascade promotes glial engulfment activity through activation of draper and phagocytic function. *Cell Death Differ* **20**, 1140–1148 (2013).

13. Ziegenfuss, J. S., Doherty, J. & Freeman, M. R. Distinct molecular pathways mediate glial activation and engulfment of axonal debris after axotomy. *Nat Neurosci* **15**, 979–987 (2012).

14. Ziegenfuss, J. S. *et al.* Draper-dependent glial phagocytic activity is mediated by Src and Syk family kinase signalling. *Nature* **453**, 935–939 (2008).

15. MacDonald, J. M. *et al.* The Drosophila Cell Corpse Engulfment Receptor Draper Mediates Glial Clearance of Severed Axons. *Neuron* **50**, 869–881 (2006).

16. Doherty, J. *et al.* PI3K Signaling and Stat92E Converge to Modulate Glial Responsiveness to Axonal Injury. *PLoS Biol* **12**, e1001985 (2014).

17. Purice, M. D. *et al.* A novel Drosophila injury model reveals severed axons are cleared through a Draper/MMP-1 signaling cascade. *Elife* **6**, e23611 (2017).

18. Musashe, D. T., Purice, M. D., Speese, S. D., Doherty, J. & Logan, M. A. Insulin-like Signaling Promotes Glial Phagocytic Clearance of Degenerating Axons through Regulation of Draper. *Cell Reports* **16**, 1838–1850 (2016).

19. Mulakkal, N. C. *et al.* Autophagy in Drosophila: From Historical Studies to Current Knowledge. *BioMed Res. Int.* **2014**, 273473 (2014).

20. Adriaenssens, E., Ferrari, L. & Martens, S. Orchestration of selective autophagy by cargo receptors. *Curr. Biol.* **32**, R1357–R1371 (2022).

21. Gohel, R., Kournoutis, A., Petridi, S. & Nezis, I. P. Molecular mechanisms of selective autophagy in Drosophila. *Int Rev Cell Mol Biol* **354**, 63–105 (2020).

22. Fang, Y., Soares, L., Teng, X., Geary, M. & Bonini, N. M. A Novel Drosophila Model of Nerve Injury Reveals an Essential Role of Nmnat in Maintaining Axonal Integrity. *Curr Biol* **22**, 590–595 (2012).

23. Neukomm, L. J., Burdett, T. C., Gonzalez, M. A., Züchner, S. & Freeman, M. R. Rapid in vivo forward genetic approach for identifying axon death genes in Drosophila. *Proc National Acad Sci* **111**, 9965–9970 (2014).

24. Bach, E. A. *et al.* GFP reporters detect the activation of the Drosophila JAK/STAT pathway in vivo. *Gene Expr Patterns* **7**, 323–331 (2007).

25. Chatterjee, N. & Bohmann, D. A Versatile ΦC31 Based Reporter System for Measuring AP-1 and Nrf2 Signaling in Drosophila and in Tissue Culture. *PLoS ONE* **7**, e34063 (2012).

26. Szabó, Á. *et al.* LC3-associated phagocytosis promotes glial degradation of axon debris after injury in Drosophila models. *Nat. Commun.* **14**, 3077 (2023).

27. Rahman, A. *et al.* GMAP is an Atg8a-interacting protein that regulates Golgi turnover in Drosophila. *Cell Rep.* **39**, 110903 (2022).

28. Nagy, P., Varga, Á., Kovács, A. L., Takáts, S. & Juhász, G. How and why to study autophagy in Drosophila: It's more than just a garbage chute. *Methods* **75**, 151–161 (2015).

29. Myllymäki, H. & Rämet, M. JAK/STAT Pathway in Drosophila Immunity. *Scand. J. Immunol.* **79**, 377–385 (2014).

30. Betz, A., Lampen, N., Martinek, S., Young, M. W. & Darnell, J. E. A Drosophila PIAS homologue negatively regulates stat92E. *Proc. Natl. Acad. Sci.* **98**, 9563–9568 (2001).

31. Nakagawa, K. & Yokosawa, H. PIAS3 induces SUMO-1 modification and transcriptional repression of IRF-1. *FEBS Lett.* **530**, 204–208 (2002).

32. Hari, K. L., Cook, K. R. & Karpen, G. H. The Drosophila Su(var)2-10 locus regulates chromosome structure and function and encodes a member of the PIAS protein family. *Genes Dev.* **15**, 1334–1348 (2001).

33. Ninova, M. *et al.* Su(var)2-10 and the SUMO Pathway Link piRNA-Guided Target Recognition to Chromatin Silencing. *Mol. Cell* **77**, 556-570.e6 (2020).

34. Bence, M. *et al.* Direct interaction of Su(var)2-10 via the SIM-binding site of the Piwi protein is required for transposon silencing in Drosophila melanogaster. *FEBS J.* **291**, 1759–1779 (2024).

35. He, L., Binari, R., Huang, J., Falo-Sanjuan, J. & Perrimon, N. In vivo study of gene expression with an enhanced dual-color fluorescent transcriptional timer. *Elife* **8**, e46181 (2019).

36. Philips, R. L. *et al.* The JAK-STAT pathway at 30: Much learned, much more to do. *Cell* **185**, 3857–3876 (2022).

37. Dostert, C. *et al.* The Jak-STAT signaling pathway is required but not sufficient for the antiviral response of drosophila. *Nat. Immunol.* **6**, 946–953 (2005).

38. Freeman, M. R., Delrow, J., Kim, J., Johnson, E. & Doe, C. Q. Unwrapping Glial Biology Gcm Target Genes Regulating Glial Development, Diversification, and Function. *Neuron* **38**, 567–580 (2003).

39. Ahn, H. J., Jeon, S.-H. & Kim, S. H. Expression of a set of glial cell-specific markers in the Drosophila embryonic central nervous system. *BMB Rep.* **47**, 354–359 (2014).

40. Alphen, B. van *et al.* Glial immune-related pathways mediate effects of closed head traumatic brain injury on behavior and lethality in Drosophila. *Plos Biol* **20**, e3001456 (2022).

41. Nagayach, A. & Wang, C. Autophagy in neural stem cells and glia for brain health and diseases. *Neural Regen. Res.* **19**, 729–736 (2023).

42. Qin, Y. *et al.* Impaired autophagy in microglia aggravates dopaminergic neurodegeneration by regulating NLRP3 inflammasome activation in experimental models of Parkinson's disease. *Brain, Behav., Immun.* **91**, 324–338 (2021).

43. Sung, K. & Jimenez-Sanchez, M. Autophagy in Astrocytes and its Implications in Neurodegeneration. *J. Mol. Biol.* **432**, 2605–2621 (2020).

44. Berglund, R. *et al.* The aging mouse CNS is protected by an autophagy-dependent microglia population promoted by IL-34. *Nat. Commun.* **15**, 383 (2024).

45. Houtman, J. *et al.* Beclin1-driven autophagy modulates the inflammatory response of microglia via NLRP3. *EMBO J.* **38**, (2019).

46. Ekas, L. A. *et al.* Characterization of a dominant-active STAT that promotes tumorigenesis in Drosophila. *Dev. Biol.* **344**, 621–636 (2010).

47. Hwang, S. P. & Lee, D. H. Autophagy mediates SUMO-induced degradation of a polyglutamine protein ataxin-3. *Anim. Cells Syst.* **21**, 169–176 (2017).

48. Han, J., Mu, Y. & Huang, J. Preserving genome integrity: The vital role of SUMO-targeted ubiquitin ligases. *Cell Insight* **2**, 100128 (2023).

49. Abed, M., Bitman-Lotan, E. & Orian, A. The Biology of SUMO-Targeted Ubiquitin Ligases in Drosophila Development, Immunity, and Cancer. *J. Dev. Biol.* **6**, 2 (2018).

50. Marmor-Kollet, H. *et al.* Spatiotemporal Proteomic Analysis of Stress Granule Disassembly Using APEX Reveals Regulation by SUMOylation and Links to ALS Pathogenesis. *Mol. Cell* **80**, 876-891.e6 (2020).

51. Lascorz, J., Codina-Fabra, J., Reverter, D. & Torres-Rosell, J. SUMO-SIM interactions: From structure to biological functions. *Semin. Cell Dev. Biol.* **132**, 193–202 (2022).

52. Pu, M., Fu, B. & Zhang, Y. J. LLPSWise - fast and accurate prediction of LLPS constituents. *bioRxiv* 2022.07.25.501404 (2022) doi:10.1101/2022.07.25.501404.

53. Cattenoz, P. B. *et al.* Temporal specificity and heterogeneity of Drosophila immune cells. *EMBO J.* **39**, e104486 (2020).

54. Zhu, H., Ludington, W. B. & Spradling, A. C. Cellular and molecular organization of the Drosophila foregut. *Proc. Natl. Acad. Sci.* **121**, e2318760121 (2024).

55. Logan, M. A. *et al.* Negative regulation of glial engulfment activity by Draper terminates glial responses to axon injury. *Nat Neurosci* **15**, 722–730 (2012).

56. Neukomm, L. J., Burdett, T. C., Gonzalez, M. A., Züchner, S. & Freeman, M. R. Rapid in vivo forward genetic approach for identifying axon death genes in Drosophila. *Proc National Acad Sci* **111**, 9965–9970 (2014).

57. Escartin, C. *et al.* Reactive astrocyte nomenclature, definitions, and future directions. *Nat. Neurosci.* **24**, 312–325 (2021).

58. Ray, A., Speese, S. D. & Logan, M. A. Glial Draper Rescues Aβ Toxicity in a Drosophila Model of Alzheimer's Disease. *J Neurosci* **37**, 11881–11893 (2017).

59. Diao, F. *et al.* Plug-and-Play Genetic Access to Drosophila Cell Types using Exchangeable Exon Cassettes. *Cell Rep.* **10**, 1410–1421 (2015).

60. Kim, M. *et al.* Mutation in ATG5 reduces autophagy and leads to ataxia with developmental delay. *eLife* **5**, e12245 (2016).

61. Tusco, R. *et al.* Kenny mediates selective autophagic degradation of the IKK complex to control innate immune responses. *Nat. Commun.* **8**, 1264 (2017).

62. Wu, J. S. & Luo, L. A protocol for dissecting Drosophila melanogaster brains for live imaging or immunostaining. *Nat Protoc* **1**, 2110–2115 (2006).

63. Andreev, V. I. *et al.* Panoramix SUMOylation on chromatin connects the piRNA pathway to the cellular heterochromatin machinery. *Nat. Struct. Mol. Biol.* **29**, 130–142 (2022).

64. Gonzalez, I., Mateos-Langerak, J., Thomas, A., Cheutin, T. & Cavalli, G. Identification of Regulators of the Three-Dimensional Polycomb Organization by a Microscopy-Based Genome-wide RNAi Screen. *Mol. Cell* **54**, 485–499 (2014).

# Fig. 1

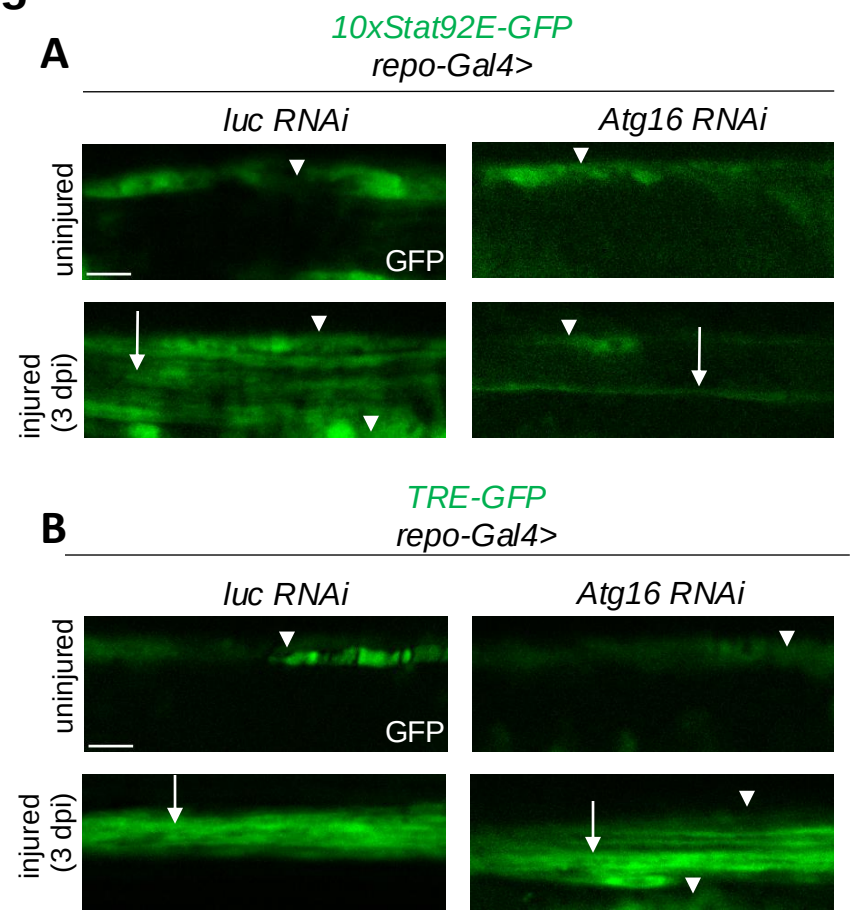
A
10xStat92E-GFP
repo-Gal4>
luc RNAi
Atg16 RNAi
uninjured
injured (3 dpi)
GFP
B
TRE-GFP
repo-Gal4>
luc RNAi
Atg16 RNAi
uninjured
injured (3 dpi)
GFP

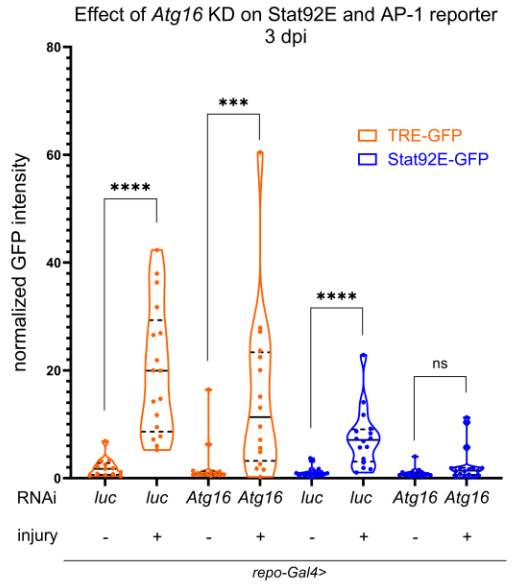
C
Effect of Atg16 KD on Stat92E and AP-1 reporter
3 dpi
normalized GFP intensity
TRE-GFP
Stat92E-GFP
****
***
****
ns
RNAi luc luc Atg16 Atg16 luc luc Atg16 Atg16
injury - + - + - + - +
repo-Gal4>

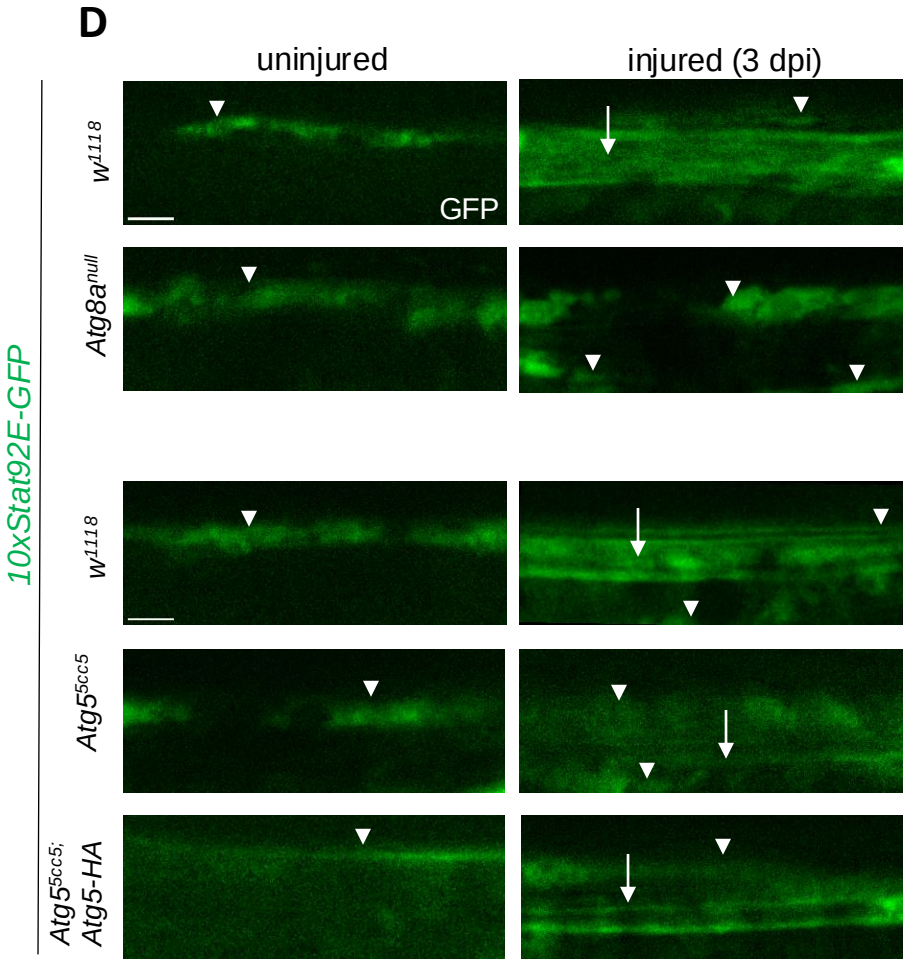
D
uninjured
injured (3 dpi)
10xStat92E-GFP
w1118
Atg8anull
w1118
Atg5cc5
Atg5cc5; Atg5-HA
GFP

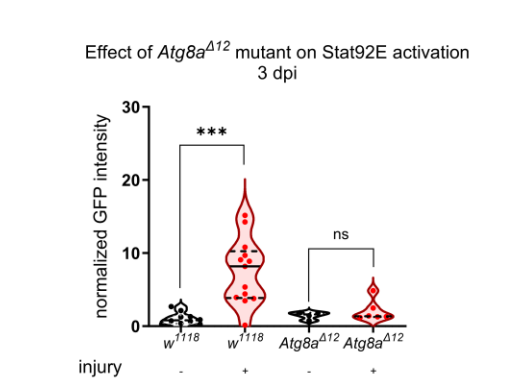
E
Effect of Atg8aΔ12 mutant on Stat92E activation
3 dpi
normalized GFP intensity
***
ns
w1118 w1118 Atg8aΔ12 Atg8aΔ12
injury - + - +

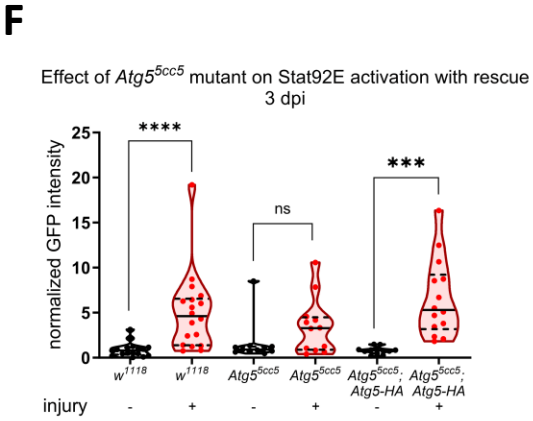
F
Effect of Atg5cc5 mutant on Stat92E activation with rescue
3 dpi
normalized GFP intensity
****
ns
***
w1118 w1118 Atg5cc5 Atg5cc5 Atg5cc5; Atg5-HA Atg5cc5; Atg5-HA
injury - + - + - +

# Fig. 2

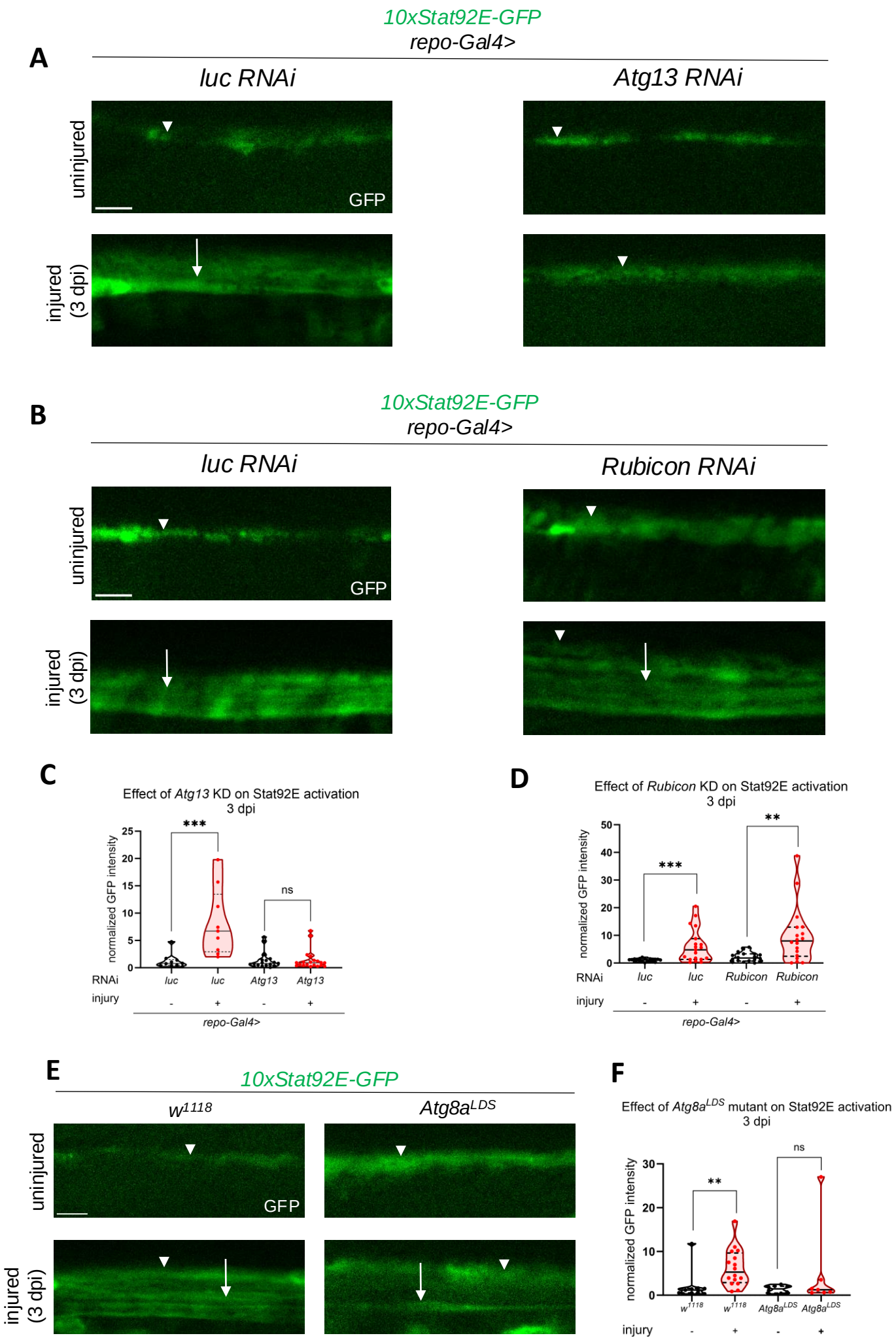
A
10xStat92E-GFP
repo-Gal4>
luc RNAi
Atg13 RNAi
uninjured
injured (3 dpi)
GFP
B
10xStat92E-GFP
repo-Gal4>
luc RNAi
Rubicon RNAi
uninjured
injured (3 dpi)
GFP
C
Effect of Atg13 KD on Stat92E activation
3 dpi
normalized GFP intensity
***
ns
RNAi
luc
luc
Atg13
Atg13
injury
-
+
-
+
repo-Gal4>
D
Effect of Rubicon KD on Stat92E activation
3 dpi
normalized GFP intensity
***
**
RNAi
luc
luc
Rubicon
Rubicon
injury
-
+
-
+
repo-Gal4>
E
10xStat92E-GFP
w1118
Atg8aLDS
uninjured
injured (3 dpi)
GFP
F
Effect of Atg8aLDS mutant on Stat92E activation
3 dpi
normalized GFP intensity
**
ns
w1118
w1118
Atg8aLDS
Atg8aLDS
injury
-
+
-
+

# Fig. 3

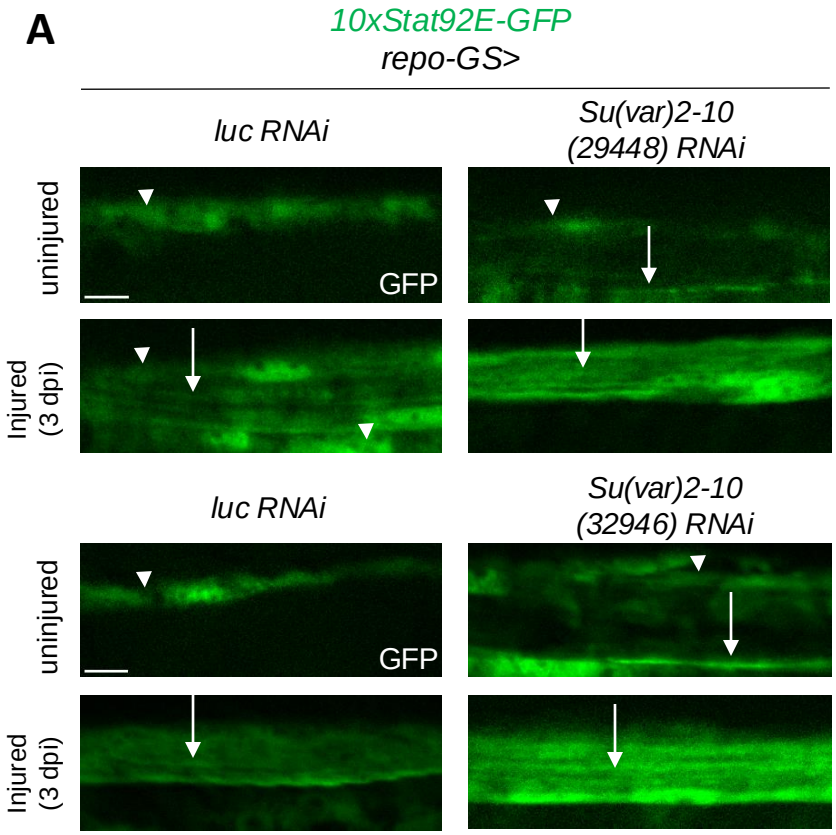
A
10xStat92E-GFP
repo-GS>
luc RNAi
Su(var)2-10 (29448) RNAi
uninjured
Injured (3 dpi)
GFP
luc RNAi
Su(var)2-10 (32946) RNAi
uninjured
Injured (3 dpi)
GFP

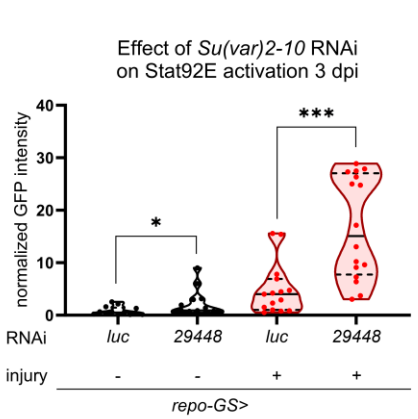
B
Effect of Su(var)2-10 RNAi on Stat92E activation 3 dpi
normalized GFP intensity
0
10
20
30
40
*
***
RNAi
luc
29448
luc
29448
injury
-
-
+
+
repo-GS>

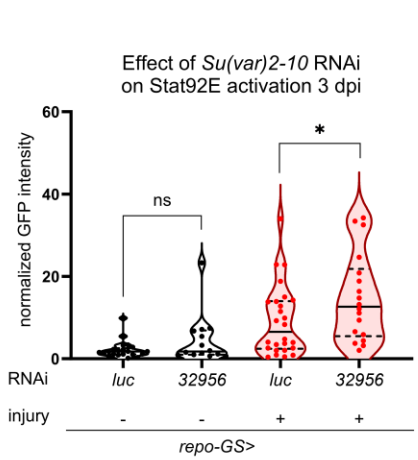
C
Effect of Su(var)2-10 RNAi on Stat92E activation 3 dpi
normalized GFP intensity
0
20
40
60
ns
*
RNAi
luc
32956
luc
32956
injury
-
-
+
+
repo-GS>

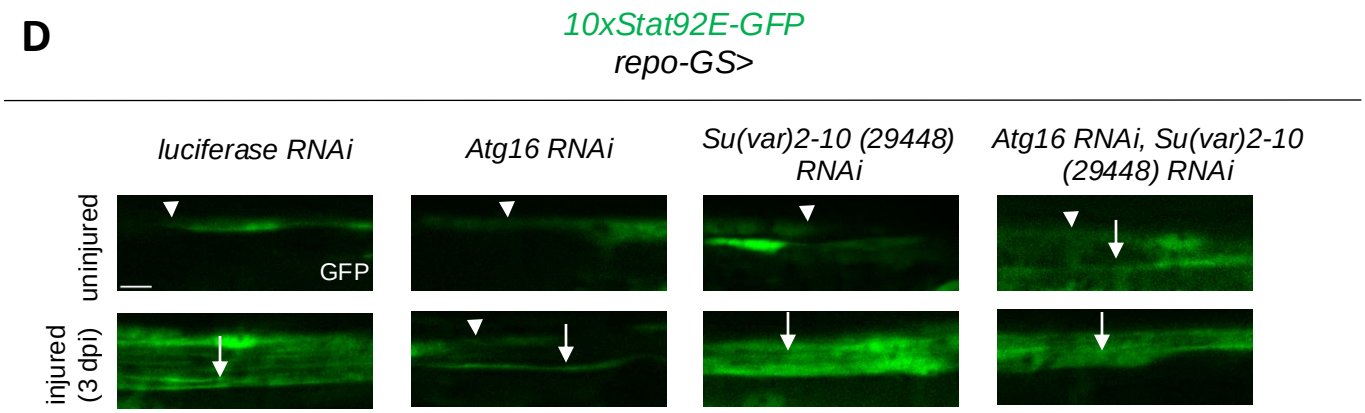
D
10xStat92E-GFP
repo-GS>
luciferase RNAi
Atg16 RNAi
Su(var)2-10 (29448) RNAi
Atg16 RNAi, Su(var)2-10 (29448) RNAi
uninjured
injured (3 dpi)
GFP

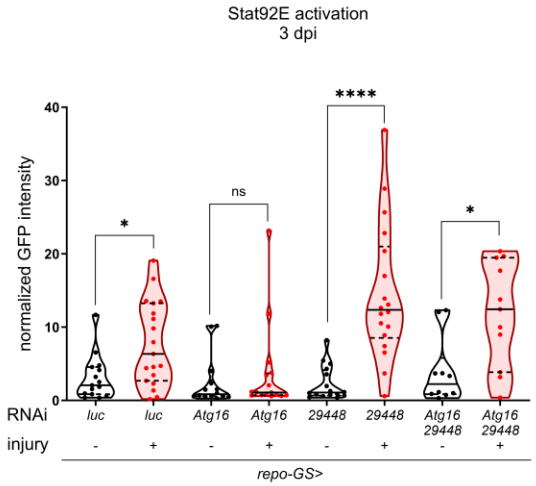
E
Stat92E activation 3 dpi
normalized GFP intensity
0
10
20
30
40
*
ns
****
*
RNAi
luc
luc
Atg16
Atg16
29448
29448
Atg16 29448
Atg16 29448
injury
-
+
-
+
-
+
-
+
repo-GS>

# Fig. 4

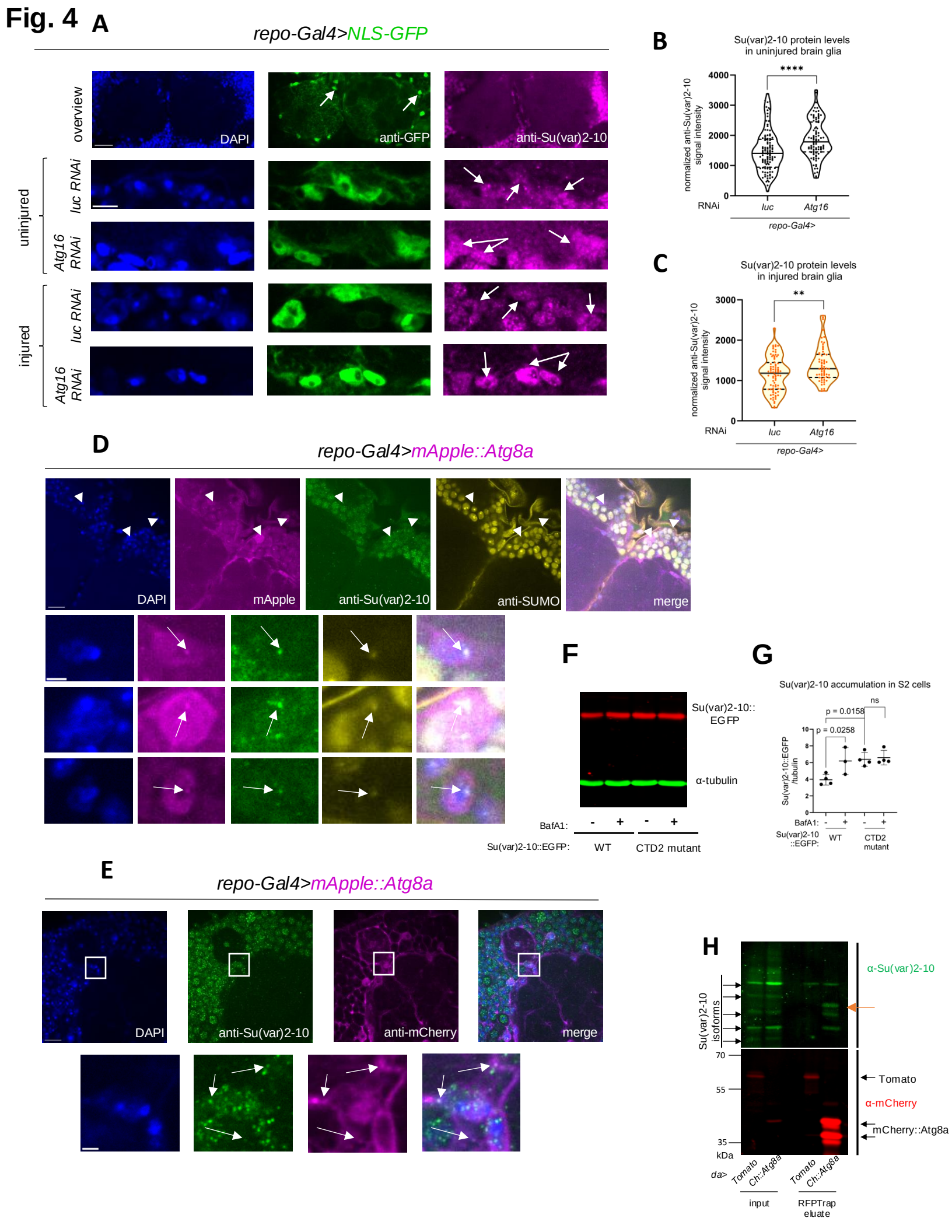
A
repo-Gal4>NLS-GFP
overview
DAPI
anti-GFP
anti-Su(var)2-10
uninjured
luc RNAi
Atg16 RNAi
injured
luc RNAi
Atg16 RNAi
B
Su(var)2-10 protein levels in uninjured brain glia
****
normalized anti-Su(var)2-10 signal intensity
4000
3000
2000
1000
0
RNAi
luc
Atg16
repo-Gal4>
C
Su(var)2-10 protein levels in injured brain glia
**
normalized anti-Su(var)2-10 signal intensity
3000
2000
1000
0
RNAi
luc
Atg16
repo-Gal4>
D
repo-Gal4>mApple::Atg8a
DAPI
mApple
anti-Su(var)2-10
anti-SUMO
merge
F
Su(var)2-10::EGFP
α-tubulin
BafA1: - + - +
Su(var)2-10::EGFP: WT CTD2 mutant
G
Su(var)2-10 accumulation in S2 cells
ns
p = 0.0158
p = 0.0258
Su(var)2-10::EGFP /tubulin
10
8
6
4
2
0
BafA1: - + - +
Su(var)2-10 ::EGFP: WT CTD2 mutant
E
repo-Gal4>mApple::Atg8a
DAPI
anti-Su(var)2-10
anti-mCherry
merge
H
Su(var)2-10 isoforms
α-Su(var)2-10
70
55
35
kDa
Tomato
α-mCherry
mCherry::Atg8a
da>
Tomato
Ch::Atg8a
Tomato
Ch::Atg8a
input
RFPTrap eluate

# Fig. 5

**A**

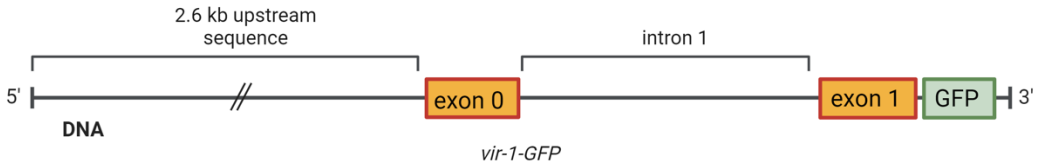


**B**

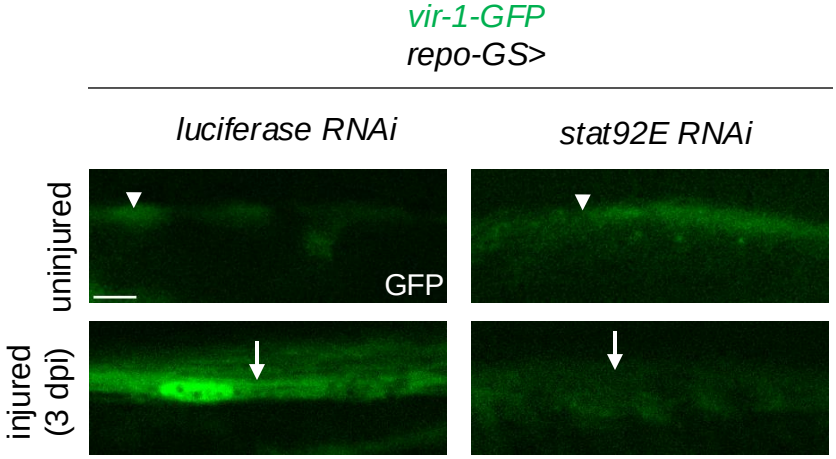


**C**

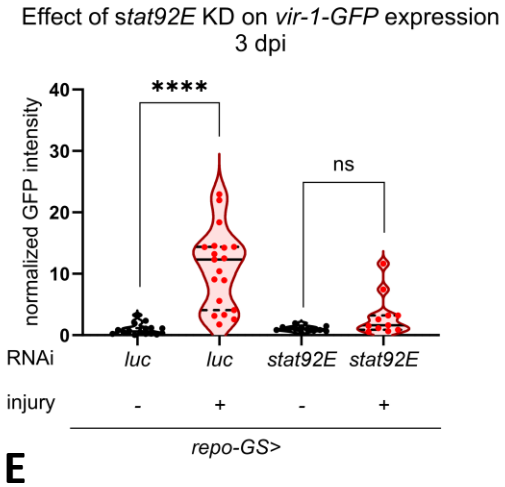


**D**

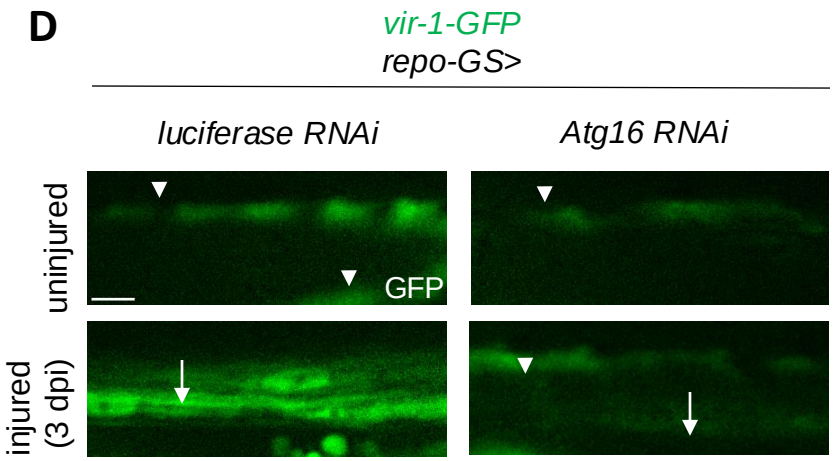


**E**

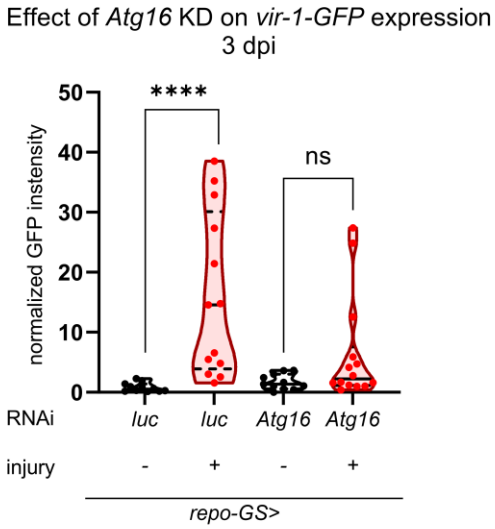


**F**

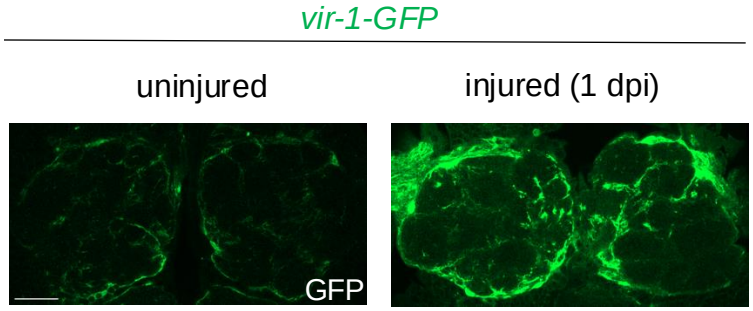


**G**

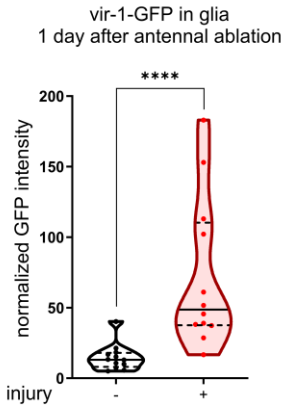

**Fig. 6**

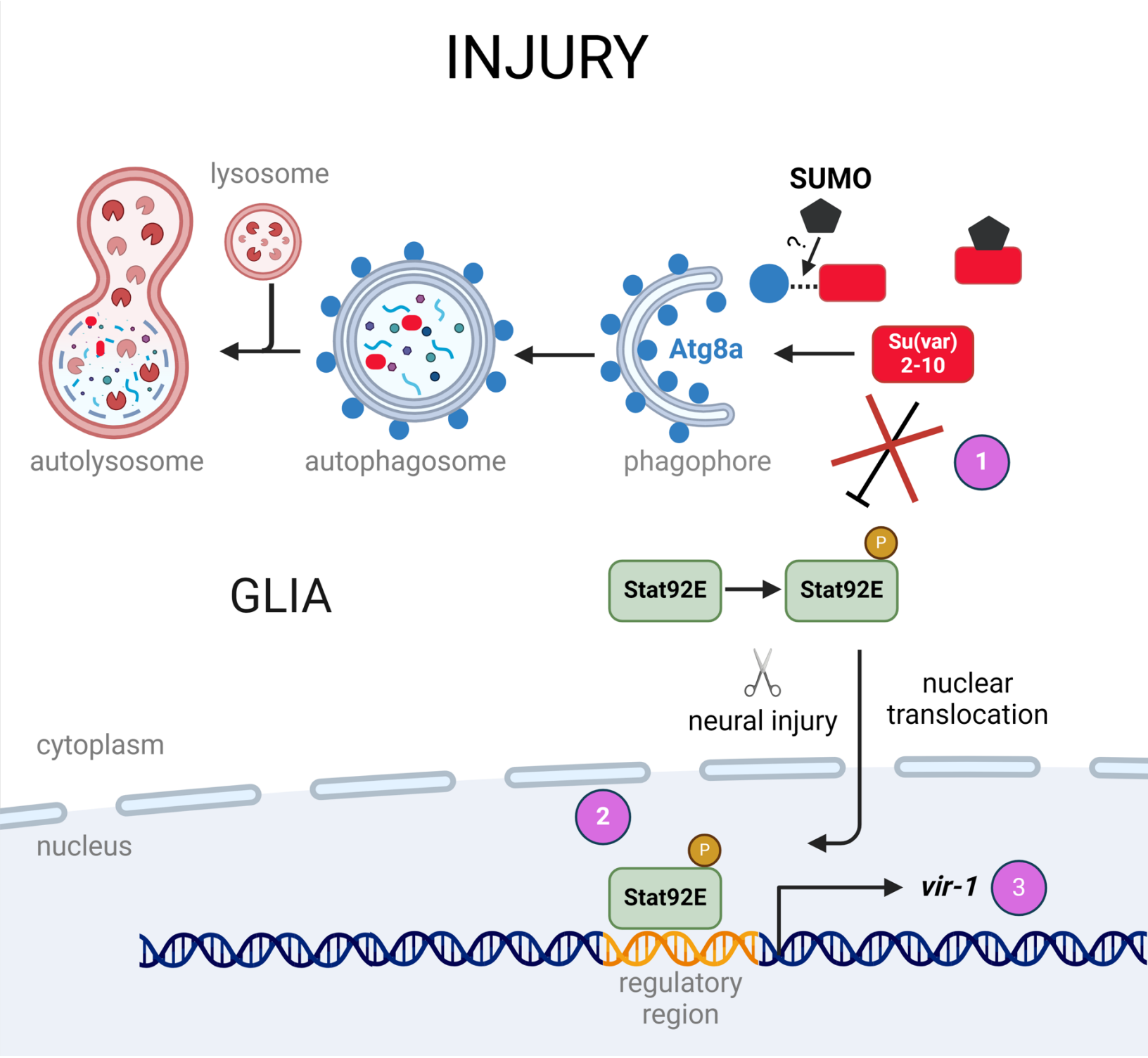
INJURY
lysosome
SUMO
?
autolysosome
autophagosome
Atg8a
phagophore
Su(var)
2-10
1
GLIA
Stat92E
P
Stat92E
neural injury
nuclear
translocation
cytoplasm
2
nucleus
P
Stat92E
vir-1
3
regulatory
region